



Research article

Optimization of 3D printing parameters in polylactic acid bio-metamaterial under cyclic bending loading considering fracture features

Ali Dadashi, Mohammad Azadi*

Research Laboratory of Advanced Materials Behavior (AMB), Faculty of Mechanical Engineering, Semnan University, Semnan, Iran

ARTICLE INFO

Keywords:

Statistical analysis
Optimization
3D printing
Polylactic acid
Bio-metamaterial
Fracture features

ABSTRACT

3D printing has become a crucial additive manufacturing technique with the applications in various industries. Fused deposition modeling (FDM) is a common additive manufacturing process that offers considerable flexibility in the component fabrication through multiple parameters, which strongly influence the properties of the produced parts. This study focused on the impact of different printing parameters on the fatigue behavior of polylactic acid (PLA). The standard samples were 3D-printed with varying speed (5, 10, and 15 mm/s), print temperature (180, 210, and 240 °C), and nozzle diameter (0.2, 0.4, and 0.6 mm). The fatigue properties were evaluated through rotating bending fatigue tests, and a model was developed based on the results with a statistical analysis. The model accuracy was validated and the interactions between the parameters were analyzed. The optimization study found that a print speed of 5 mm/s, print temperature of 210 °C, and nozzle diameter of 0.2 mm were optimal. The fracture surfaces were also examined using a scanning electron microscopy, revealing the presence of crazing despite the brittle behavior of PLA.

1. Introduction

A production process consists of operations that bring the geometry shape to a material with desired properties in order to achieve the proper function of an object, which is a combination of geometry and its properties. In additive manufacturing, the desired shape is acquired by successive addition of material; therefore, the parts can be combined into more complex shaped products [1].

It helps to create structural and artificial materials with unusual properties in nature, known as metamaterials [2]. The name is chosen to emphasize and recognize their purpose, which is achieving properties “beyond” the limitations of traditional materials [3]. Extensive research has been done on designing a periodic structure as a unit cell to achieve the desired properties. Clausen et al. [4] achieved a controllable Poisson ratio by topology optimization and also provided the ability to absorb energy. Sepehri et al. [5] introduced snowflake-inspired and spider-web unit cells to the regular geometries to control and enhance locally resonant bandgaps in metamaterials of periodic triangular and hexagonal topologies. By combining an indium tin oxide (ITO) resonator with a poly-ether-ether-ketone (PEEK) dielectric using a melting sediment modeling technique, Yang et al. [6] proposed a lightweight meta-structure that, in addition to greater electromagnetic absorption bandwidth, has excellent mechanical, thermal, and physical properties.

* Corresponding author.

E-mail address: m_azadi@semnan.ac.ir (M. Azadi).

<https://doi.org/10.1016/j.heliyon.2024.e26357>

Received 28 August 2023; Received in revised form 9 February 2024; Accepted 12 February 2024

Available online 16 February 2024

2405-8440/Â© 2024 The Authors. Published by Elsevier Ltd. This is an open access article under the CC BY-NC license (<http://creativecommons.org/licenses/by-nc/4.0/>).

Despite the unique performance of metamaterials, their reliability is still a challenge [7] because the parameters of the additive manufacturing process can affect the properties of the parts. Abeykoon et al. [8] examined the impact of 3D printing parameters on printed parts. Higher filling density increased the elastic modulus. Polylactic acid (PLA) parts had an elastic modulus of 1538 MPa at 100% of filling density. A printing speed of 90 mm/s resulted in the highest elastic modulus for PLA. The optimal printing temperature for PLA was found to be 215 °C. Alafaghani and Qattawi [9] studied the effects of fused deposition modeling (FDM) printing parameters on the dimensional accuracy and mechanical properties. Lower printing temperature, thinner layers, lower infill density, and hexagonal infill pattern improved the dimensional accuracy. FDM components are usually larger than CAD models. Higher printing temperature and infill density increased the strength with the optimal layer thickness and triangular infill pattern. Changing the infill pattern and increasing the layer thickness enhanced the ductility. PLA filaments were used in studies by Sandhu et al. [10] to estimate the effect of FDM process parameters on the surface roughness of the prints. Optimal parameters were cubic infill pattern, raster angle of 60°, and layer thickness of 0.16 mm. Moreover, mechanical properties varied with minimum strength of 23–35 MPa, maximum strength of 26–39 MPa, and maximum elongation of 5%–6%. The optimal parameters resulted in the best mechanical properties [11]. Travieso-Rodriguez et al. [12] studied PLA-wood composites produced by FDM with varying parameters. Wood-reinforced PLA showed a weak fatigue resistance. The honeycomb filling pattern with specific parameters had the longest fatigue lifetime. Patil et al. [13] introduced a multi-objective optimization algorithm for FDM printing of PLA parts. The triangle pattern, 70% of infill density, printing speed of 100 mm/h, and layer thickness of 0.2 mm were identified as the optimal parameters based on the surface roughness, printing time, and consumable filament length.

Because of the versatility of the FDM manufacturing technique, it is essential to optimize and design the polymers to properly fulfill the mechanical objectives, such as fatigue properties and damage mechanisms [14]. As stated by the American Society for Testing and Materials (ASTM), the fatigue process is a localized and progressive permanent change in the structure, which occurs in a material subjected to cyclic loading that may lead to crack nucleation and propagation or complete fracture after an adequate number of cycles [15]. The fluctuating stress and strain conditions in various applications affect the material strength and durability [16]. Gomez et al. [17] found that the layer thickness affected the fatigue lifetime of PLA in rotating bending fatigue tests. PLA specimens with a layer height of 0.3 mm, 0.5 mm of nozzle diameter, and 75% of infill density exhibited increased the fatigue resistance. When printed at 45° of orientation, PLA results showed the improved fatigue strength, compared to 0° and 90° of print directions, along with the enhanced strain energy [18]. Ezeh and Susmel [19] analyzed the crack growth in notched PLA specimens, made with FDM. The fatigue stress caused the irregular crack propagation along the filament orientation, leading to filament cracking, debonding between filaments, and debonding between layers. Zhang et al. [20] investigated the influence of printing orientation on the fatigue, tensile, and creep properties of 3D-printed ABS parts. The highest mechanical properties were observed at 0° of orientation, with a modulus of elasticity of about 1.8 GPa and an ultimate strength of 224 MPa. The best creep resistance was found in 90° of print direction with $k = 0.2$. Additionally, increasing the load from 30 N to 60 N significantly decreased the average rotary fatigue lifetime from 3796 cycles to 128 cycles. Lee and Huang [21] investigated the impact of cyclic conditions on the strain energy in FDM-printed ABS-P430 and ABS-P400. The printed ABSplus data illustrated the improved energy absorption before fracture and similar tensile strength. ABSplus-P430 exhibited increased isotropy compared to ABS-P400 and failed at approximately 1000 cycles at 40% of ultimate stress. The influence of different building parameters (printing speed, nozzle diameter, layer height, and infill density) on the fatigue lifetime of cylindrical specimens printed by the FDM method from ABS material was studied by Domingo-Espin et al. [22] according to a design of experiments. The filling density has the most significant effect on the fatigue life of the samples made of ABS material.

Uncontrolled anisotropy in 3D-printed parts will cause problems [23,24]; therefore, understanding the role of fatigue in polymers printed with the FDM process would be difficult, and few pieces of research have been devoted to the fatigue behavior of these materials [25]. However, it can be controlled using optimal parameters [26]. This study investigates the influences of the nozzle diameter, print temperature, and print speed on the fatigue lifetime of 3D-printed polylactic acid (PLA) specimens trying to understand how the manufacturing parameters affect the properties. In this research, innovations include.

- 1 Impact of individual printing parameter variations as well as the interactions,
- 2 Experimental analysis using rotating bending fatigue tests and exploring the failure mechanisms, particularly their influence by variations in printing parameters,
- 3 Understanding the fatigue resistance and parameter optimization,
- 4 Statistical and regression analysis based on experimental data in order to optimize printing parameters for best part durability and performance.

The study uses the experimentation, data analysis, and modeling to enhancing the performance and durability of 3D-printed objects. The research is to examine the influence of different print parameters on the fatigue properties of 3D printed PLA biomaterial through experiments. In addition to this exploration, a regression analysis was performed, which resulted in the development of a predictive model for estimating the fatigue lifetime. The model was validated and its reliability was examined through the statistical analysis. This study not only broadens understanding of the interactions between printing parameters and fatigue properties; but also offers a practical tool for reliably predicting the fatigue lifetime of PLA biomaterials, which can help improve and ensure the quality of 3D printing.

Therefore, the steps taken in this research were as follows.

- The standard geometry was designed, and specimens were manufactured using selected parameters.
- The fatigue behavior is analyzed by the S–N fatigue diagram.

- The statistical analysis was performed, and a regression model was introduced according to the test data.
- The fracture surfaces were investigated in order to determine the failure mechanisms as well as the impact of print parameters on the microscopic behavior of the material.

2. Materials and procedures

2.1. Experimental Factors

The strength of the parts printed with additive manufacturing depends on the printing parameters. To clarify the parameters affecting the fatigue lifetime, some of them are shown in the Ishikawa diagram in Fig. 1.

The underlined parameters in Fig. 1 had been examined in previous research by the authors [27–29], while print speed, print temperature, and nozzle diameter were examined in this study and are indicated with rectangular boxes. The levels of these variable parameters in terms of coded factor units (+1/-1) are summarized in Table 1. The other parameters were considered constant in all samples based on Table 2. The value of each parameter was selected according to the literature [13,30–43], as well as the physical specifications of the printer.

Accordingly, the range of parameters is specified in the last column of Tables 1 and 2. The samples were named after the print parameters in order to make them easily referred to (Fig. 2). For example, the specimen printed at 210 °C as print temperature, with a nozzle diameter of 0.6 mm, and print speed of 10 mm/s is displayed as “PLA-0.6-10-210”.

The print temperature, which is the operating temperature of the extruder, provides appropriate extrusion as well as cohesion in the workpiece [28]. It is essential to heat the polymeric material to a temperature between the melting point (T_m) and the glass transition temperature (T_g), where the material starts to soften; therefore, the layered deposition of filament would be possible. At higher temperatures, the material cannot maintain its shape, and at lower temperatures, it is not soft enough to be extruded [44]. Accordingly, the print temperature has been chosen in the range of 180–240 °C. Printing speed affects print quality and print time. At low speeds, printing time increases which cause higher manufacturing cost. In contrast, at very high speeds, dimensional accuracy decreases as the device starts to vibrate. In addition, filament injection problems may also occur at high printing speeds. Therefore, 5, 10, and 15 mm/s were considered as printing speeds. The diameter of the nozzle is another factor affecting the printing time and quality. Considering the fact that nozzles with diameters of 0.1–1.0 mm are available, nozzles with diameters of 0.2, 0.4, and 0.6 mm were used.

Fatigue tests were performed at various levels of stress to obtain the fatigue properties according to the behavior of the material in each printing condition. Therefore, regression analysis has been carried out with four input factors and the fatigue lifetime as a response, which are reported in Table 3 and Table 4.

2.2. Test specimens

According to ISO 1143 standard [45], the fatigue specimen can be loaded with one, two, or four points like a cantilever. Based on the conditions mentioned in this standard, the ratio of large diameter to small diameter (D/d) should be at least 1.732, and the radius of the sample arc, r , should have a radius greater than or equal to $5d$. The sample was designed as shown in Fig. 3, with units reported in millimeters, and then sliced based on building parameters.

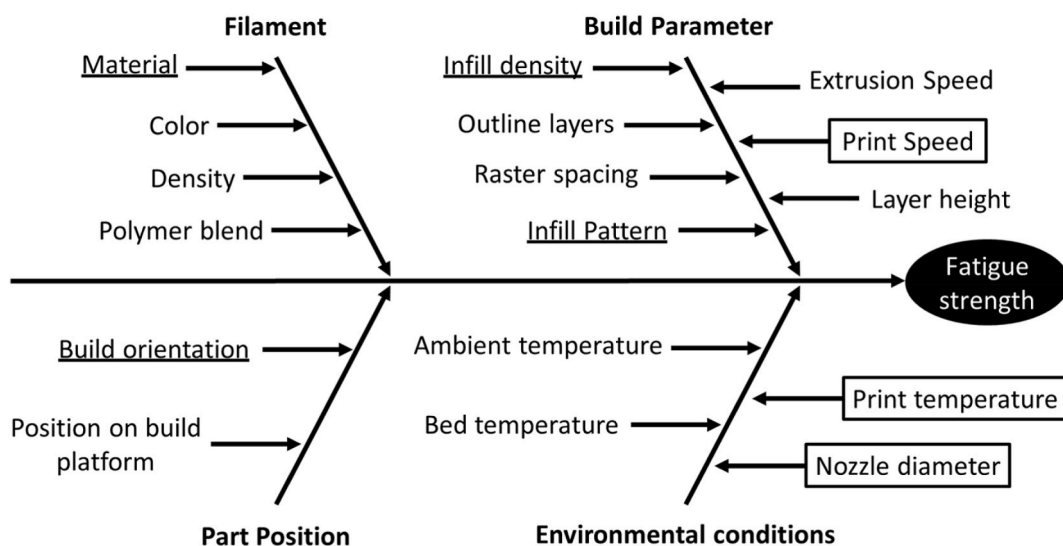


Fig. 1. The Ishikawa diagram of parameters affecting the fatigue strength.

Table 1
The variable parameters in 3D printing.

Parameter	Dimension	Level			Range
		-1	0	1	
Speed of 3D Printing	mm/s	5	10	15	7.5–100
Temperature of 3D Printing	°C	180	210	240	175–240
Diameter of Nozzle	mm	0.2	0.4	0.6	0.3–0.8

Table 2
The constant parameters in 3D printing.

Parameter	Dimension	Value	Range
Thickness of Layer	mm	0.2	0.02–0.3
Perimeters	–	2	2–6
Top and Bottom Solid Layer	–	1	–
Fill Pattern	–	Rectilinear	Different
Speed of Travel	mm/s	30	Different
Platform Temperature	°C	30	20–110
Direction of 3D Printing	–	Horizontal	Different
Infill Percentage	%	60	10–100
Outline Overlap	%	15	0–100



Fig. 2. Naming samples based on the parameters used for printing.

Table 3
The report of the final response.

Name	Units	Observations	Minimum	Maximum	Mean	Std. Dev.
Fatigue Lifetime	cycle	105	1200	1.50E+06	1.17E+05	3.16E+05

Table 4
The report of the design factors.

Factor	A	B	C	D
Name	Nozzle diameter	Print speed	Print temperature	Stress level
Units	mm	mm/s	°C	MPa
Type	Numeric	Numeric	Numeric	Numeric
SubType	Continuous	Continuous	Continuous	Continuous
Minimum	0.2	5	180	2.5
Maximum	0.6	15	240	17.5
Coded Low	-1 ↔ 0.20	-1 ↔ 5.00	-1 ↔ 180.00	-1 ↔ 2.50
Coded High	+1 ↔ 0.60	+1 ↔ 15.00	+1 ↔ 240.00	+1 ↔ 17.50
Mean	0.4229	9.90	210.00	8.19
Std. Dev.	0.1625	3.92	23.90	3.33

2.3. 3D printing

The interactions between software, hardware, and material properties in an optimized print process are complex [46]. Therefore, a fused deposition modeling 3D printer device was developed with three axes in which the extruder moves on the X–Y plane with a belt driving system and the build platform moves by a lead screw driving system on the Z axis (Fig. 4). This machine is able to print parts with a maximum dimension of $550 \times 600 \times 700 \text{ mm}^3$ and an accuracy of $50 \mu\text{m}$ and $40 \mu\text{m}$ on the X–Y and Z axes, respectively, owing to the driving mechanism of the axes. It includes the NEMA 17 stepper motor with two phases and a step-angle of 1.8° . Furthermore, a driver with the ability to adjust micro step resolutions (1/16, 1/8, 1/4, 1/2, Full) by controlling the electrical current and switches were used. The Marlin firmware, an open-source program, was developed according to the machine specifications. The firmware

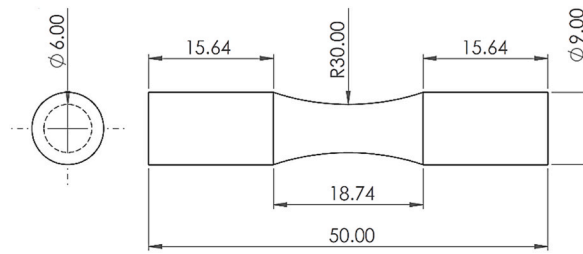


Fig. 3. The standard geometry of the fatigue sample at millimetric scale.

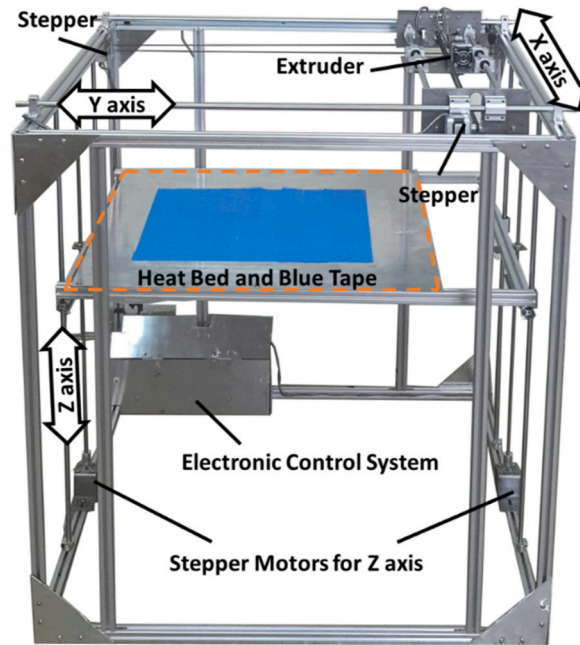


Fig. 4. The 3D printer device for additive manufacturing of testing samples based on the FDM technique.

converts G-code commands into a machine format. Simplify3D software is utilized to specify 3D printing parameters and prepare the G-code from the 3D file (STL). As shown in Fig. 4, in order to enhance the adhesion of the layers to the work surface as well as make it easier to separate the printed component from the printer, the surface of the printing bed was also covered with Blue Tape, which is a type of fireproof adhesive tape. A transparent-colored PLA (the YouSu company) with a filament diameter of 1.75 mm was used to feed

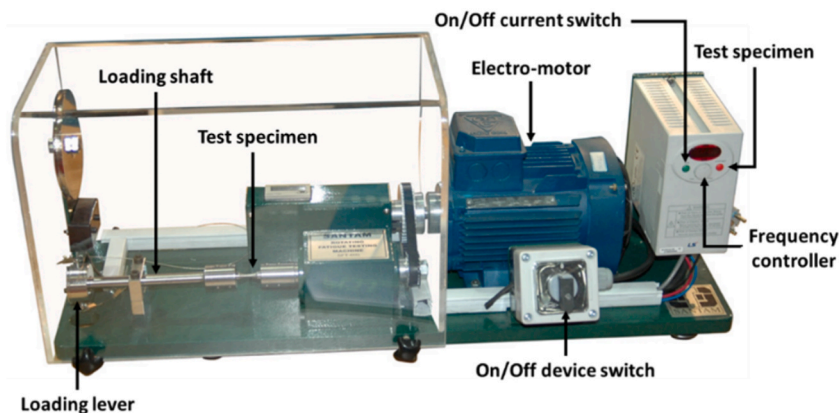


Fig. 5. The rotary bending fatigue testing device (SFT-600 Santam Company).

the MK8 extruder.

2.4. Fatigue Testing

The fatigue experiment was done at room temperature (30 °C) with a high-cycle rotary bending test machine developed by Santam company (Fig. 5). The loading condition was fully reversed, in which the stress ratio equals -1 ($R_\sigma = \frac{\sigma_{min}}{\sigma_{max}} = -1$). The failure criterion was a complete fracture of specimens before 1.5×10^6 cycles. It means that the fatigue tests were interrupted after the specimens endured 1.5×10^6 cycles with no failure, which are called “Run-out” specimens. The loading frequency in all the fatigue tests is 100 Hz, equivalent to 6000 rpm. The S–N curve (also known as the Wöhler curve), which is the result of fatigue tests, demonstrates the logarithm of the lifetime or the number of reversals to failure versus applied stress amplitude.

A linear trend line was fitted to the S–N curve resulting from the test results to find the relation between the fatigue lifetime (N_f) and the stress amplitude (σ_a). By comparing the power equation with the Basquin expression in Equation (1), two material properties, namely the fatigue strength exponent (b) and the fatigue strength coefficient (σ'_f), will be obtained [47].

$$\sigma_a = \sigma'_f (2N_f)^b \tag{1}$$

2.5. Statistical Analysis

Data analysis and modeling should be performed after every experimental work, based on Fig. 6. A regression analysis makes it possible to investigate the effect of print parameters on fatigue lifetime. The cubic regression assumes the response variable, i.e., fatigue lifetime can be modeled by a three-degree polynomial formulation. The results were evaluated by P-value measurement and the coefficient of determination (R^2). A smaller P-value shows greater statistical significance. In other words, the relation between the response variable and a term is significant when the P-value is less than 0.05.

In addition, R^2 can be used to check the accuracy of the model [49]. Based on Equation (2), the parameter is the model explanation of variation around the mean [50].

$$R^2 = \frac{SS_{residual}}{SS_{total}} = 1 - \frac{SS_{error}}{SS_{total}} \tag{2}$$

By considering, SS as the sum of squares obtained by the differences between the overall average and the amount of variation, SS_{total} is the model sum of squares, and $SS_{residual}$ is the residual sum of squares, which can be obtained from Equation (3) [50].

$$SS_{residual} = SS_{LOF} + SS_{PE} \tag{3}$$

In Equation (3), SS_{LOF} stands for the sum of squares related to lack of fit that is the amount of miss in the prediction by the model. SS_{PE} is also the sum of squares related to the pure error and shows an evaluation of the effect contributed by the error associated with repeatability. In addition, R^2_{adj} and R^2_{pred} can also be used to verify the model quality [50], based on Equations (4) and (5).

$$R^2_{adj} = 1 - \frac{MS_{res}}{MS_{tot}} \tag{4}$$

$$R^2_{pred} = 1 - \frac{PRESS}{SS_{tot}} \tag{5}$$

The adjusted coefficient of determination, R^2_{adj} , is the model explanation of variation around the overall response average (Mean). Increasing the number of terms in the model causes R^2_{adj} to be decreased if the additional terms do not add value. It is while the predicted coefficient of determination, R^2_{pred} , is the model explanation of variation in new data. In Equation (4), MS is the mean square and can be calculated based on dividing SS (the sum of squares) by N (the degrees of freedom). Then, the fitness of design points is determined by the predicted residual error sum of squares ($PRESS$) [50].

$$PRESS = \sum_{i=1}^n (y_i - \hat{y}_i)^2 \tag{6}$$

In Equation (6), y_i and \hat{y}_i are the actual and predicted values, respectively.

Model confirmation is an important step for assessing model adequacy, according to Fig. 6. Ignoring this step can result in a model that underperforms when used in future applications. It also provides reliable extrapolations of statistical results. Accordingly, some data were randomly selected to confirm and validate the model. Although there are many different recommendations for the number of



Fig. 6. The stages of experimental research from statistical point of view [48].

tests required for confirmation, very little justification is provided [51]. In general, the more conformation tests, the more probability of detecting an issue in the prediction process, whereas they give only a small improvement. In addition, excess confirmation runs could reduce the model efficiency by reducing the data used in the model fit. Therefore 75% of the total results were used to analyze and fit the model. The remaining 25% were used for validation. Table 5 is related to the resulting analysis of variance (ANOVA).

In the last stage of regression analysis, the design points were subjected to numerical optimization in order to determine the optimal parameters. For this purpose, constraints could be considered discontinuous functions (Equation (7)) [50].

$$\begin{cases} g_j(X) = y_j(X) - U_j; & \text{for } y_j > U_j \\ g_j(X) = 0; & \text{for } L_j \leq y_j \leq U_j \\ g_j(X) = L_j - y_j(X); & \text{for } y_j < L_j \end{cases} \tag{7}$$

In Equation (7), X is the vector of design variables over the optimization space (x_i for $i = 1:n$), y is the response to be optimized, and L and U are the lower and upper bounds as constraints (U_j, L_j for $j = 1:m$). Therefore, with the help of a penalty approach, the m constraints system could be solved as an unconstrained problem [50].

$$\min\left\{f(X) + p \sum_j g_j(X)\right\} \tag{8}$$

In Equation (8), $f(X)$ is the objective function. For a minimization problem $f(X) = y(X)$ and in a maximization problem $f(X) = -y(X)$. p is a penalty parameter that is positive (begins from 1 and increases by iteration with a factor of 100 until 15 iterations) for $j = 1:m$.

In order to assess how well the variables satisfied the goals for the responses, the desirability function approach was used. For each response $y_n(X)$, a desirability function $d_n(y_n)$ assigns numbers between 0 and 1 to the possible values of y_n [50]. By considering \hat{y} as fitted response models, when a response is to be maximized, the individual desirability function can be calculated based on Equation (9).

Table 5
The analysis of variance in the cubic regression model.

Source	Sum of Squares	DF	Mean Square	F-value	P-value	Coefficient
Model	54.0500	31	1.7400	28.3900	<0.0001	-
A-Nozzle diameter	2.7400	1	2.7400	44.5600	<0.0001	-0.5038
B-Print speed	0.8839	1	0.8839	14.3900	0.0003	0.3041
C-Print temperature	1.7900	1	1.7900	29.1500	<0.0001	-0.4825
D-Stress level	2.5200	1	2.5200	41.0700	<0.0001	-1.3500
AB	1.3700	1	1.3700	22.3600	<0.0001	0.2863
AC	0.0319	1	0.0319	0.5193	0.4735	-0.0406
AD	0.4586	1	0.4586	7.4700	0.0079	0.2776
BC	0.3186	1	0.3186	5.1900	0.0257	0.1677
BD	0.0146	1	0.0146	0.2384	0.6268	-0.0756
CD	0.0636	1	0.0636	1.0400	0.3123	-0.1909
A ²	4.3800	1	4.3800	71.2900	<0.0001	0.6348
B ²	0.9605	1	0.9605	15.6400	0.0002	-0.2603
C ²	0.1071	1	0.1071	1.7400	0.1908	-0.0997
D ²	0.2636	1	0.2636	4.2900	0.0418	0.4164
ABC	0.0071	1	0.0071	0.1162	0.7342	-0.0197
ABD	0.3067	1	0.3067	4.9900	0.0285	0.3074
ACD	0.1727	1	0.1727	2.8100	0.0978	0.2389
BCD	0.2282	1	0.2282	3.7200	0.0578	-0.3572
A ² B	0.5836	1	0.5836	9.5000	0.0029	-0.2268
A ² C	0.7387	1	0.7387	12.0300	0.0009	0.2779
A ² D	0.0182	1	0.0182	0.2966	0.5877	-0.0888
AB ²	8.85E-06	1	8.85E-06	0.0001	0.9905	-0.0008
AC ²	0.0833	1	0.0833	1.3600	0.2481	0.0825
AD ²	0.0002	1	0.0002	0.0027	0.9584	0.0095
B ² C	0.1190	1	0.1190	1.9400	0.1682	0.1027
B ² D	0.0120	1	0.0120	0.1950	0.6601	0.0690
BC ²	0.6248	1	0.6248	10.1700	0.0021	-0.2498
BD ²	0.1442	1	0.1442	2.3500	0.1298	-0.3533
C ² D	0.1186	1	0.1186	1.9300	0.1689	0.2564
CD ²	0.0022	1	0.0022	0.0358	0.8505	-0.0561
D ³	0.1118	1	0.1118	1.8200	0.1815	0.4033
Intercept	-	1	-	-	-	3.7837
Residual	4.4800	73	0.0614	-	-	-
Lack of Fit	3.9300	59	0.0666	1.6800	0.1413	-
Pure Error	0.5542	14	0.0396	-	-	-
Cor Total	58.5300	104	-	-	-	-

$$d(\hat{y}_n) = \begin{cases} 0 & \hat{y}_n < L_n \\ \left(\frac{\hat{y}_n - L_n}{T_n - L_n}\right)^s & L_n \leq \hat{y}_n \leq T_n \\ 1.0 & T_n < \hat{y}_n \end{cases} \quad (9)$$

where n is the number of responses and s is the importance of the response (equals to 1.0 by default). L_n , U_n and T_n are as the lower, upper and a large value for response, respectively. $d_n(y_n) = 0$ represents a completely undesirable value of y_n and $d_n(y_n) = 1$ represents a completely desirable or ideal response value [50]. The individual desirabilities are then combined using the geometric mean (Equation (10)), which gives the overall desirability D ,

$$D = (d_1(y_1) \times d_2(y_2) \times \dots \times d_n(y_n))^{\frac{1}{n}} \quad (10)$$

If any of the responses or factors fall outside their desirability range, the overall function becomes zero [50].

2.6. Analysis of surface failures

The selected fracture surface of fatigue specimens was examined by a Zeiss field-emission scanning electron microscopy (FE-SEM), the model of Sigma 300-HV, after preparation by gold sputtering in order to create a conductive golden layer on the samples. The failure mechanism was analyzed by performing imaging with different magnifications.

3. Results and discussion

3.1. Specimen Fabrication

After designing the standard geometry, the corresponding G-code was extracted based on print parameters. The time it takes to print samples can be an effective parameter in determining the cost of printing and varies according to the printing speed as well as the diameter of the selected nozzle. Therefore, the print times in different modes are summarized in Table 6.

Since the samples were printed horizontally, the printed parts require support material to support the overhang regions and prevent the print layers from falling. Due to the cylindrical geometry, a Raft-type support layer is also taken into account to provide the appropriate adhesion of the primary layers to the printing bed, as shown in Fig. 7-a.

In order to remove all support material from the part and improve the surface quality of printed samples at the connection surfaces to the support structure, 120-grit sandpaper and then 400-grit one were used as surface finishing (Fig. 7-b).

3.2. Fatigue Behaviors

As explained in section 2.4, the high-cycle rotating-bending fatigue test was performed with a frequency of 100 Hz at room temperature, according to the ISO 1143 standard [45]. In order to compare the results, the S–N curves related to different temperatures in specified print speeds and nozzle diameters were provided (Fig. 8, Fig. 9, and Fig. 10). Notably, raw data are available in previous publications by the authors [27,28].

Moreover, based on the conducted studies in Advanced Material Behavior Laboratory at Semnan University, three data sets are included in all the graphs. The slicing parameters related to these results are summarized in Table 7, based on experiences in the research laboratory of Advanced Materials Behavior (AMB), at the Faculty of Mechanical Engineering, Semnan University, Semnan, Iran. The accuracy of the fatigue tests, as well as the reliability of the results, can be concluded from them. The obtained scatter-band and also the data trend are comparable.

As a preliminary analysis, some fatigue results had high scattering and were considered out of scatter-band data. It could be attributed to defects that occurred within the fabrication process. Such defects cause stress concentration areas and decrease fatigue lifetime. These data are omitted in the S–N diagram [27]. Moreover, the run-out samples, which were suspended after 1.5 million cycles, were specified with a horizontal arrow to show the continuity of the test procedure.

In Fig. 8-a-c, the lifetime of 3D-printed specimens using the nozzle with a nozzle diameter of 0.2 mm was decreased with the increase of the print speed, especially at higher stress levels, i.e., in the print speed of 15 mm/s. Therefore, the lifetime of the samples at the stress level of 12.5 MPa is less than the vertically printed samples. According to Fig. 8-b, samples printed at 210 °C nozzle temperature with the speed of 10 mm/s, slightly improved the fatigue properties compared to a printing speed of 5 mm/s in the same

Table 6
The printing time based on the nozzle diameter and the print speed.

3D printing speed	Nozzle diameter		
	0.2 mm	0.4 mm	0.6 mm
5 mm/s	2:16'	1:53'	0:53'
10 mm/s	1:09'	0:37'	0:27'
15 mm/s	0:46'	0:25'	0:19'

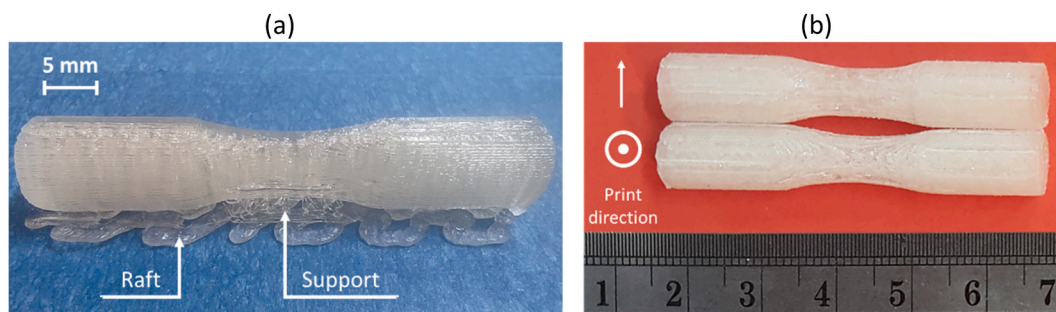


Fig. 7. The geometry of (a) as-built sample and (b) finished 3D-printed specimen.

printing conditions. In addition, increasing the print speed reduces the slope of the graph (the fatigue strength exponent), thus affecting the low-cycle behavior. The behavior of these samples is almost the same as AMB LAB 2 conditions; therefore, the fitted curve in the samples printed at 5 mm/s of the speed completely follows the corresponding trend of AMB LAB 2 conditions.

According to Fig. 9-a-c, in the samples printed with the nozzle diameter of 0.4 mm, the fatigue lifetime of the samples first improved and then reduced with increasing the printing speed. In contrast, the behavior at high temperatures was utterly different, and the fatigue lifetime under high-stress levels was decreased continuously by increasing the printing speed. Additionally, the rate of lifetime changes is more intense in high stresses. The slope was almost similar at different print speeds. The fatigue strength of the samples printed with a 0.4 mm nozzle diameter was generally lower than the specimens 3D-printed using a nozzle with 0.2 mm of the diameter; however, the fatigue lifetime in the case of printing speed equal to 10 mm/s, at 210 °C as the print temperature is higher than other print conditions. According to Fig. 9-a, samples printed using 0.4 mm of the nozzle diameter with 5 mm/s of 3D printing speed and print temperature equal to 240 °C have the lowest lifetime compared to all samples. Based on the fractography analysis, the presence of defects, such as particles or protrusions, in the printed samples could be the cause of lower fatigue lifetime.

In Fig. 10-a-c, the effect of the nozzle diameter on fatigue lifetime was slightly changed in the case of 0.6 mm nozzle diameter. Accordingly, the behavior of the samples printed at high temperature and high speed with a 0.6 mm nozzle diameter was better than the specimens 3D-printed with the nozzle diameter of 0.4 mm. Specimens printed at 180 °C as nozzle temperature tolerated more cycles to failure. Although the fatigue behavior at low print temperature decreased with increasing print speed, the fatigue properties of the printed samples improved at high extruder temperature by increasing print speed. On the other hand, increasing the print speed with the nozzle diameter equal to 0.6 mm improves the low cycle behavior of the material.

In general, the fatigue life increased by decreasing the nozzle diameter due to the denser structure and higher resolution. This is while a larger nozzle diameter results in interlayer cohesion [34] but lower surface quality [52]. However, it would be better to investigate the impact of nozzle diameter along with the thickness of the layer [53]. The effect of the speed depends on the nozzle diameter, and fatigue properties decreased by increasing the nozzle temperature. Therefore, the samples printed at 240 °C as the nozzle temperature had the lowest lifetime in most of the test conditions. This could be attributed to the overflow of the deposited layer caused by the temperature close to the melting point of the material [39].

Comparing the results of the studies that examined the influence of the process parameters showed that the effect of parameters on different properties was different. For example, the higher print speed improved tensile properties due to fast and proper bonding between layers and reduced print time in PLA samples. It is reported that temperature does not affect tensile properties [54]. Optimum parameters in ABS-enhanced PLA printing were obtained with a nozzle temperature of 215 °C, a print speed of 90 mm/s, and a filling of 100% [8]. The tensile strength of both PEEK and PEI materials first decreased and then was increased by increasing the nozzle temperature. But the tensile strength of 3D-printed PEEK was higher compared to PEI, and the variation range was small [55].

The findings of this study hold the substantial significance within the field of both additive manufacturing and materials science. By examining the influences of different 3D printing parameters on the fatigue behavior of PLA, the results provided a valuable understanding of how to optimize the mechanical properties of 3D-printed objects. These insights can be instrumental in the development of more durable and reliable components across various industries. Additionally, the S–N diagrams offer a robust framework for the future research in materials science and additive manufacturing. It provides the foundation for enhanced quality control and the utilization of 3D printing with PLA in real-world applications, ultimately advancing the potential to produce high-performance and resilient materials.

3.3. Regression Analysis

A regression model approach was used to illustrate the interaction between response (Fatigue lifetime) and input parameters (Print speed, Print temperature, Nozzle diameter, and Stress level). This regression analysis can also predict the response in different combinations of process parameter and their optimum level.

After randomly selecting 75% of the data, a base 10 logarithmic transformation was applied to the response variable and the cubic model was fitted to design parameters. Based on the P-value from the ANOVA table (Table 5), there were four main effects (*A*, *B*, *C*, and *D*) that were significant. In addition, there are 27 interaction effects where 10 terms (*AB*, *AD*, *BC*, *A*², *B*², *D*², *ABD*, *A*²*B*, *A*²*C*, *BC*²) had a P-value less than 0.05 and can be evaluated as significant terms. The model F-value of 28.39 also indicates a significant model.

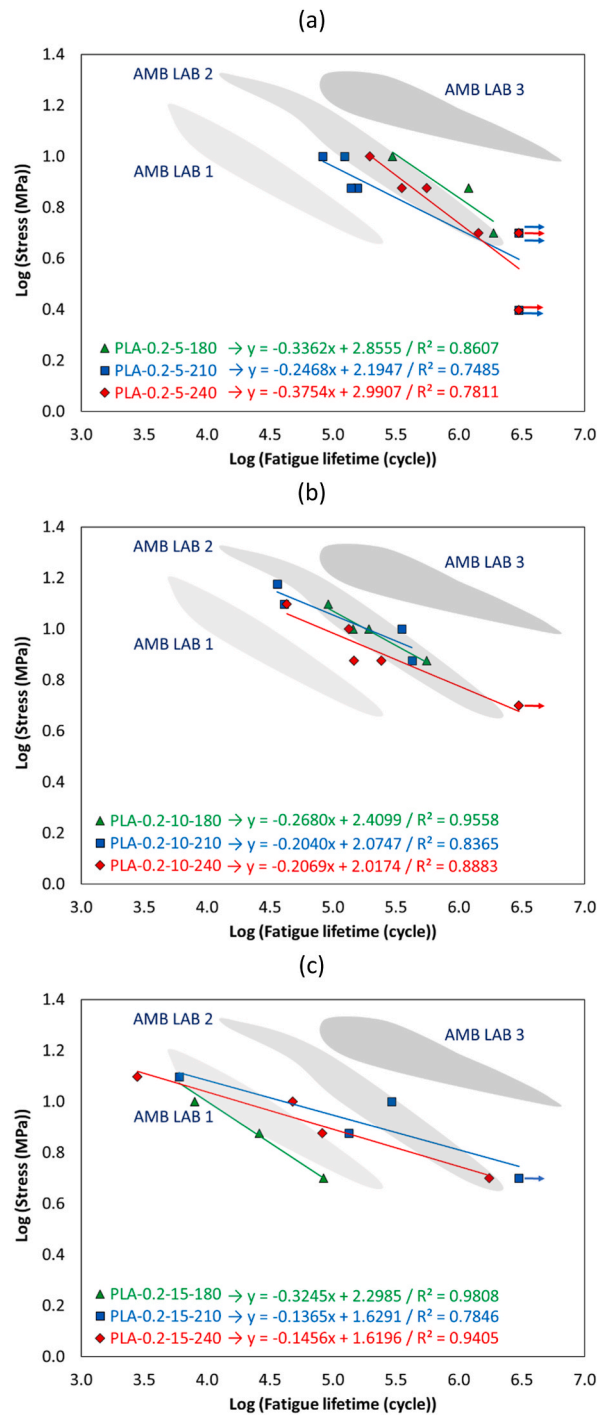


Fig. 8. The S-N curves for PLA specimens, 3D-printed with 0.2 mm of the nozzle diameter.

Moreover, only a 0.01% chance could be considered for the occurrence of such F-value because of noise. However, the Lack of Fit F-value of 1.68 is not effective compared to the pure error, and there is a 14.13% chance that such a large value could occur because of noise. It is favorable for lack of fit to be non-significant and shows a good choice of variables. The cubic model equation in terms of coded factors is mentioned in Equation (11).

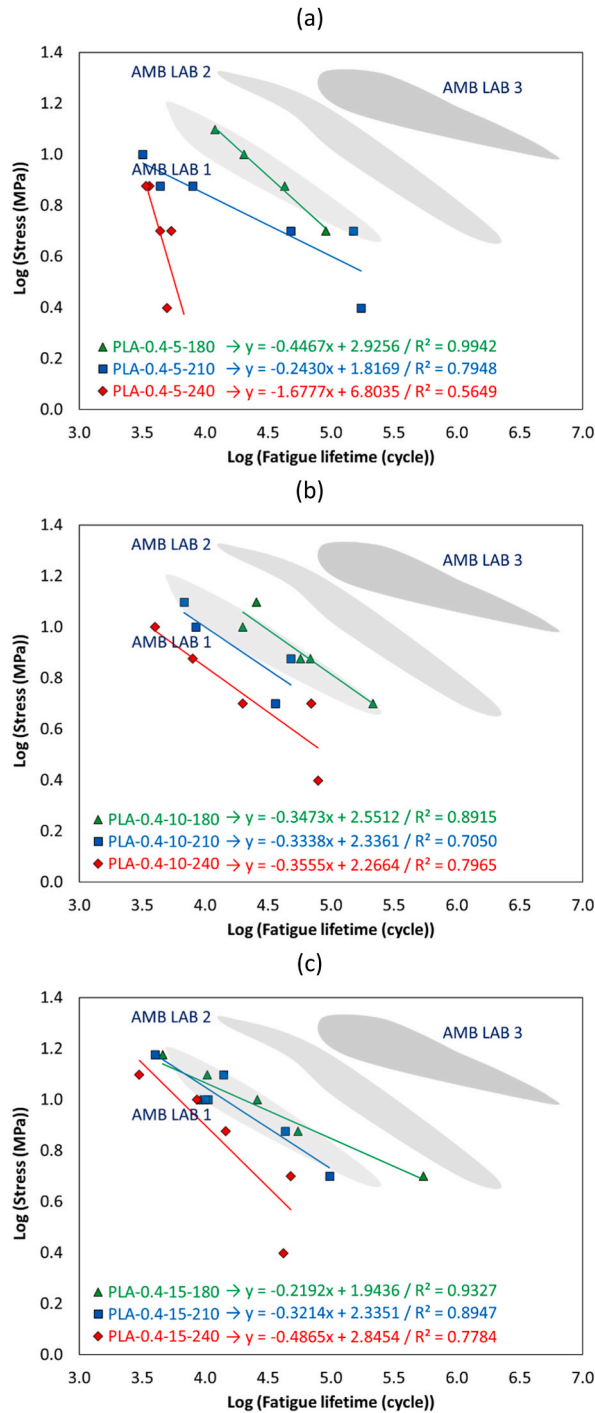


Fig. 9. The S–N curves for PLA specimens, 3D-printed with 0.4 mm of the nozzle diameter.

$$\begin{aligned} \log_{10}(N_f) = & 3.780 - 0.504A + 0.304B - 0.483C - 1.350D + 0.286AB - 0.041AC + 0.278AD + 0.168BC - 0.076BD \\ & - 0.191CD + 0.635A^2 - 0.260B^2 - 0.100C^2 + 0.416D^2 - 0.020ABC + 0.307ABD + 0.239ACD - 0.357BCD - 0.227A^2B + 0.278A^2C \\ & - 0.089A^2D - 0.001AB^2 + 0.083AC^2 + 0.010AD^2 + 0.103B^2C + 0.069B^2D - 0.250BC^2 - 0.353BD^2 + 0.256C^2D - 0.056CD^2 \\ & + 0.403D^3 \end{aligned}$$

(11)

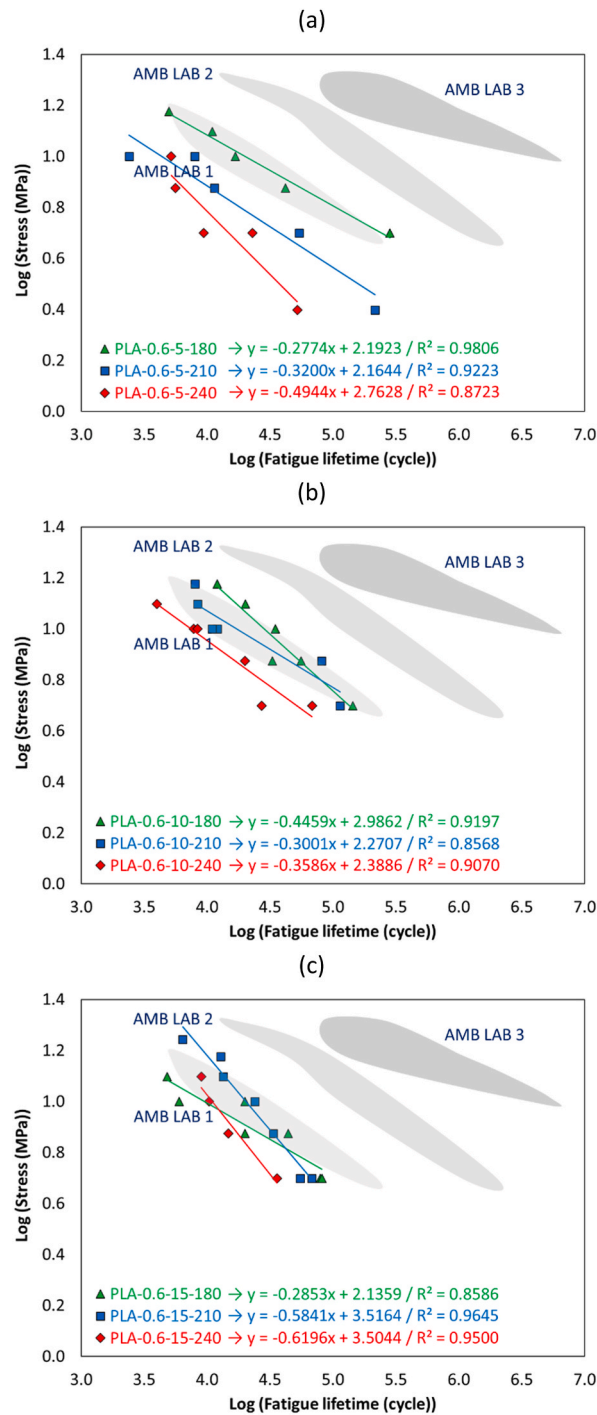


Fig. 10. The S–N curves for PLA specimens, 3D-printed with 0.6 mm of the nozzle diameter.

N_f is fatigue lifetime and A , B , C , and D are nozzle diameter, print speed, print temperature, and stress level, respectively. This equation is helpful to identify the relative impact of each term by comparing the coefficients. The R^2 value of 92.34% was suitable for result prediction. Moreover, R_{pred}^2 of 81.83% is in acceptable agreement with the R_{adj}^2 value of 89.09%; since the difference is less than 20%.

When the average of the data is equal to zero and the standard deviation is equal to one, the data distribution is normal. In order to check the assumption of normal distribution of residuals, the residual plots were inspected visually, according to Fig. 11.

The Normal Plot of Residuals (Fig. 11-a) follows a straight line and confirms the assumption of normal distribution of the residuals.

Table 7
3D printing factors for PLA in this work (© Research Laboratory of AMB, 2022).

Types of Characteristics	Parameters	AMB Lab 1	AMB Lab 2	AMB Lab 3
Physical Characteristics	Color of Filament	Black	Black	White
	Fill Pattern	Rectangular	Rectangular	Honeycomb
	3D Printing Direction	Vertical	Horizontal	Horizontal
	Infill Percentage (%)	50	50	75
	Perimeter	3	3	3
Size Characteristics	Top and Bottom Solid Layers	3	3	3
	Diameter of Nozzle (mm)	0.4	0.4	0.5
	Diameter of Filament (mm)	1.75	1.75	1.75
Thermal Characteristics	Thickness of Layer (mm)	0.15	0.15	0.20
	3D Printing Temperature (°C)	200	200	210
	Bed Temperature (°C)	60	60	50
Speed Characteristics	3D Printing Speed (mm/s)	50	50	50
	Speed of Travel (mm/s)	60	60	80

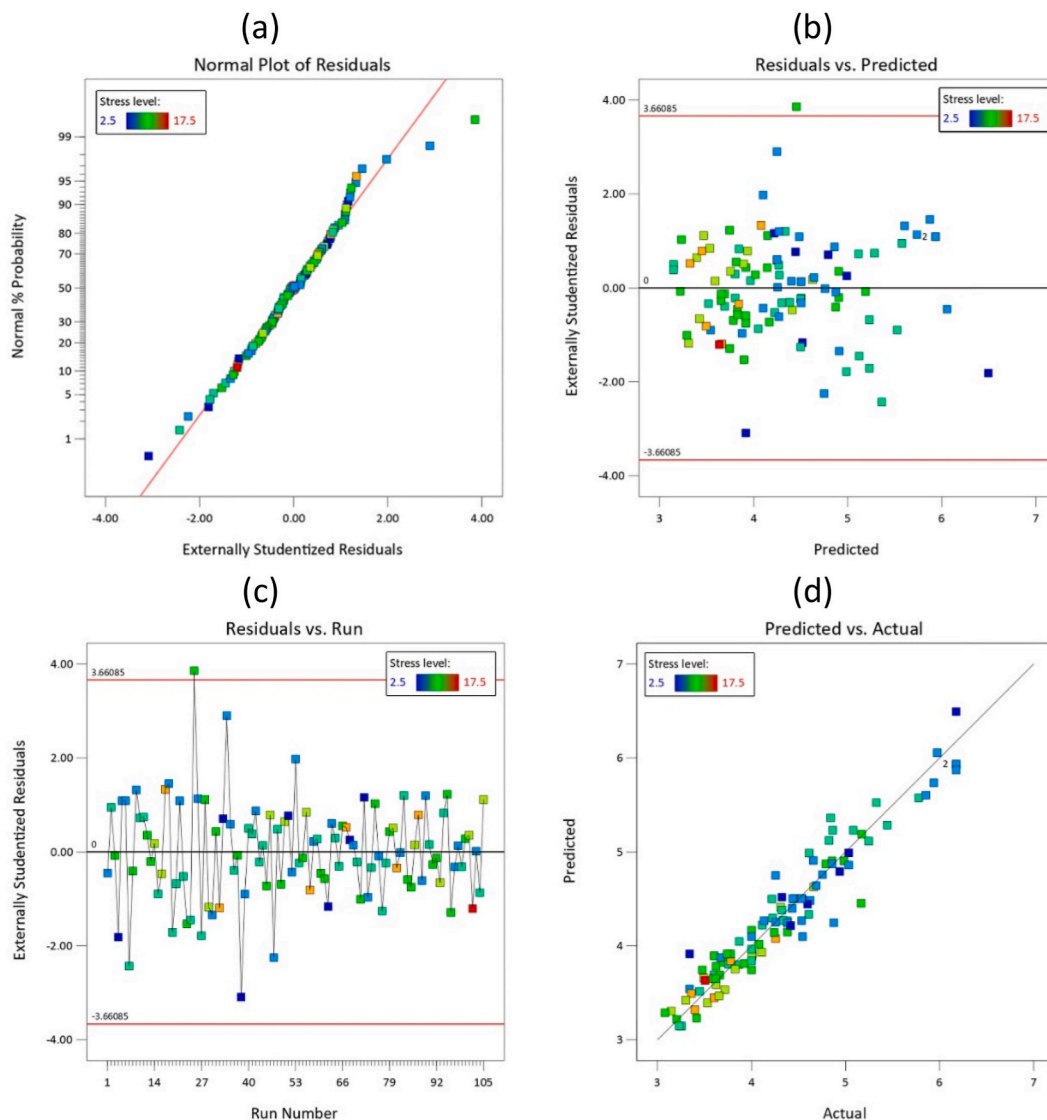


Fig. 11. Residual plots including (a) normal plots, (b) residuals versus predicted values, (c) residuals versus run order, and (d) predicted versus the actual value of fatigue lifetime.

The residuals versus ascending predicted response values plot (Fig. 11-b) confirms the assumption of stable variance based on the random distribution of the plot. The random scatter of the residuals versus the experimental run order plot (Fig. 11-c) shows the independence of the time in the model predictive performance. In this plot, externally studentized residuals are calculated by dividing each raw residual by an estimated standard deviation. The standard deviation is obtained by removing the corresponding data point, allowing for normalization with respect to that point. It can be concluded from the linear trend of the predicted versus the actual graph of response values (Fig. 11-d), that the model fits well.

To find the impact of each parameter on the fatigue lifetime, the interaction plots of two-by-two parameters, at the intermediate level of other parameters, were summarized in Fig. 12.

Accordingly, there was a crossover interaction between nozzle diameter and print speed. The main influence of the nozzle diameter and print temperature is also indicated in Fig. 12. In addition, Fig. 12 shows how the print temperature and stress level can change the effect of print speed similarly. It can be seen that the stress level can change the fatigue lifetime. Still, it is not enough to have evidence of the interaction between stress level and nozzle diameter in this population. The nozzle diameter interacted with the stress level. The effect of each parameter on the fatigue lifetime is depicted in Fig. 13-a-f through 3D surface plots and the corresponding 2D contour plot.

At the final stage of regression analysis, the remaining 25% of the results were used to confirm the model accuracy. Fatigue life prediction with the presented cubic model had an average error of 8.06%, the highest and lowest error being 26.52% and 0.81%, respectively. According to the scatter-band diagram in Fig. 14, all the data were in the range of 25X. Meanwhile, the 3X and 2X scatter-bands covered 91% and 88% of the data, respectively. Thus, the model provides a reasonable estimation of the response.

The validation process involved the use of random experimental results. The high R^2 value and the low average error in predicting fatigue lifetime suggested that the model was capable of producing accurate results. Additionally, the scatter-band diagram showed that the data points were consistently within an acceptable range, confirming the model reliability. Nevertheless, a larger dataset could

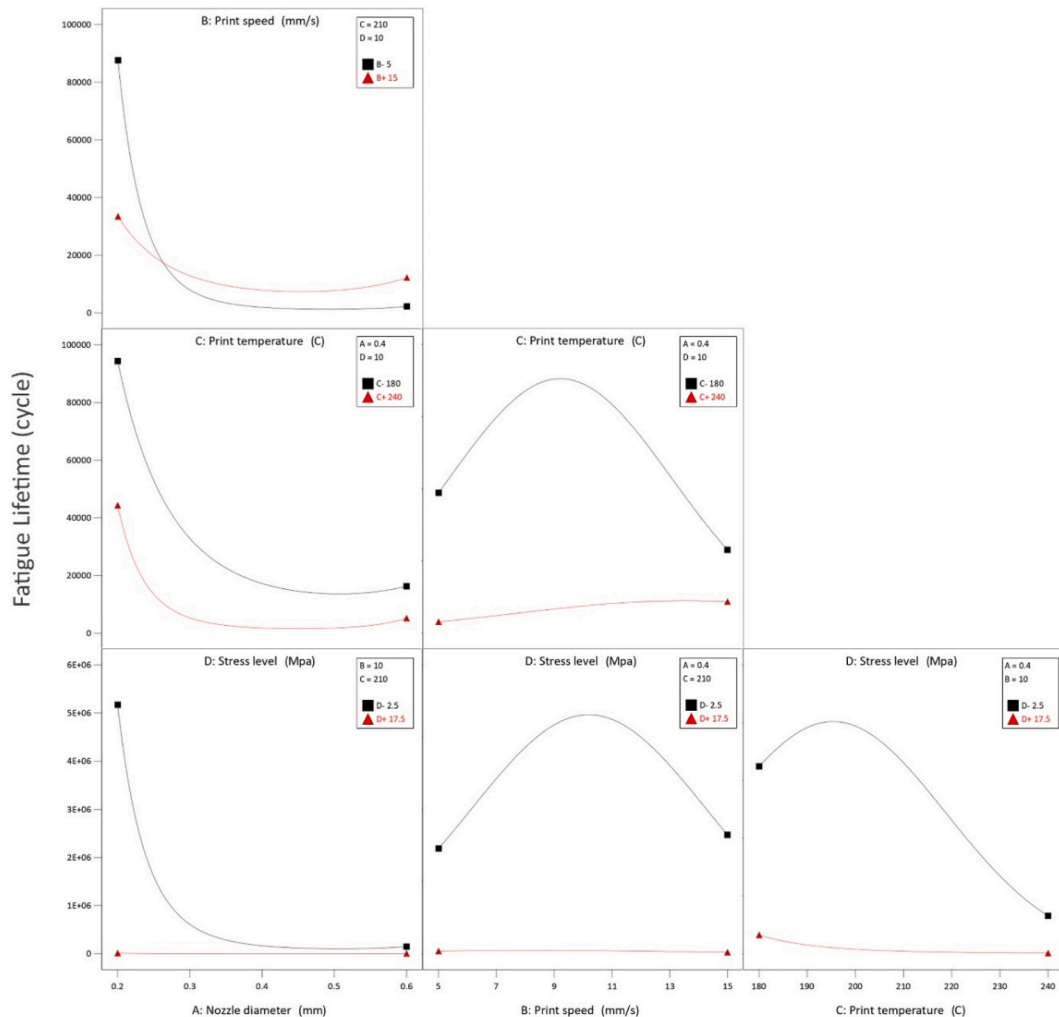


Fig. 12. The interaction plots of variable parameters and their effect on the fatigue lifetime.

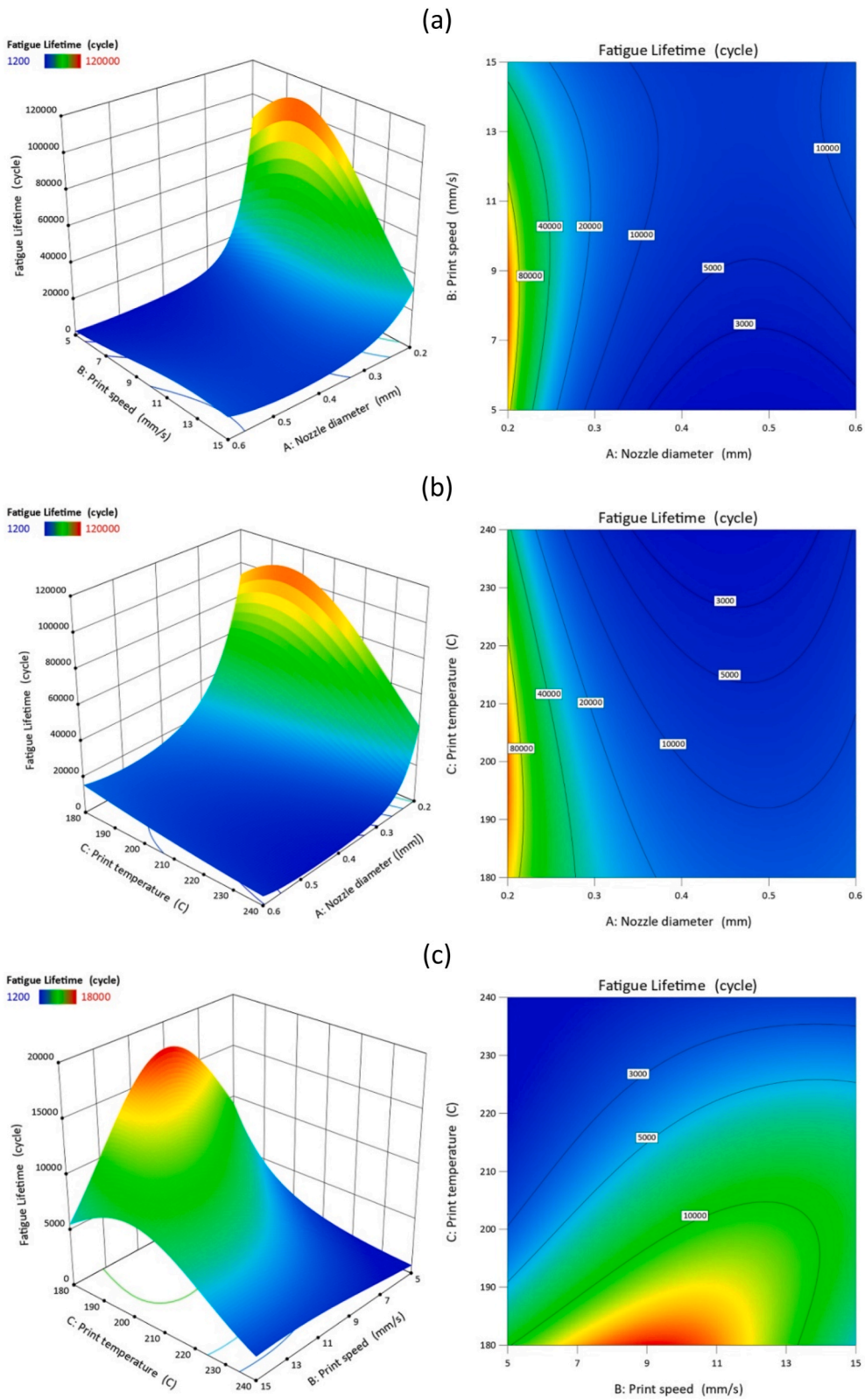


Fig. 13. 3D surface plots (left) and 2D contour plots (right) of effecting parameters.

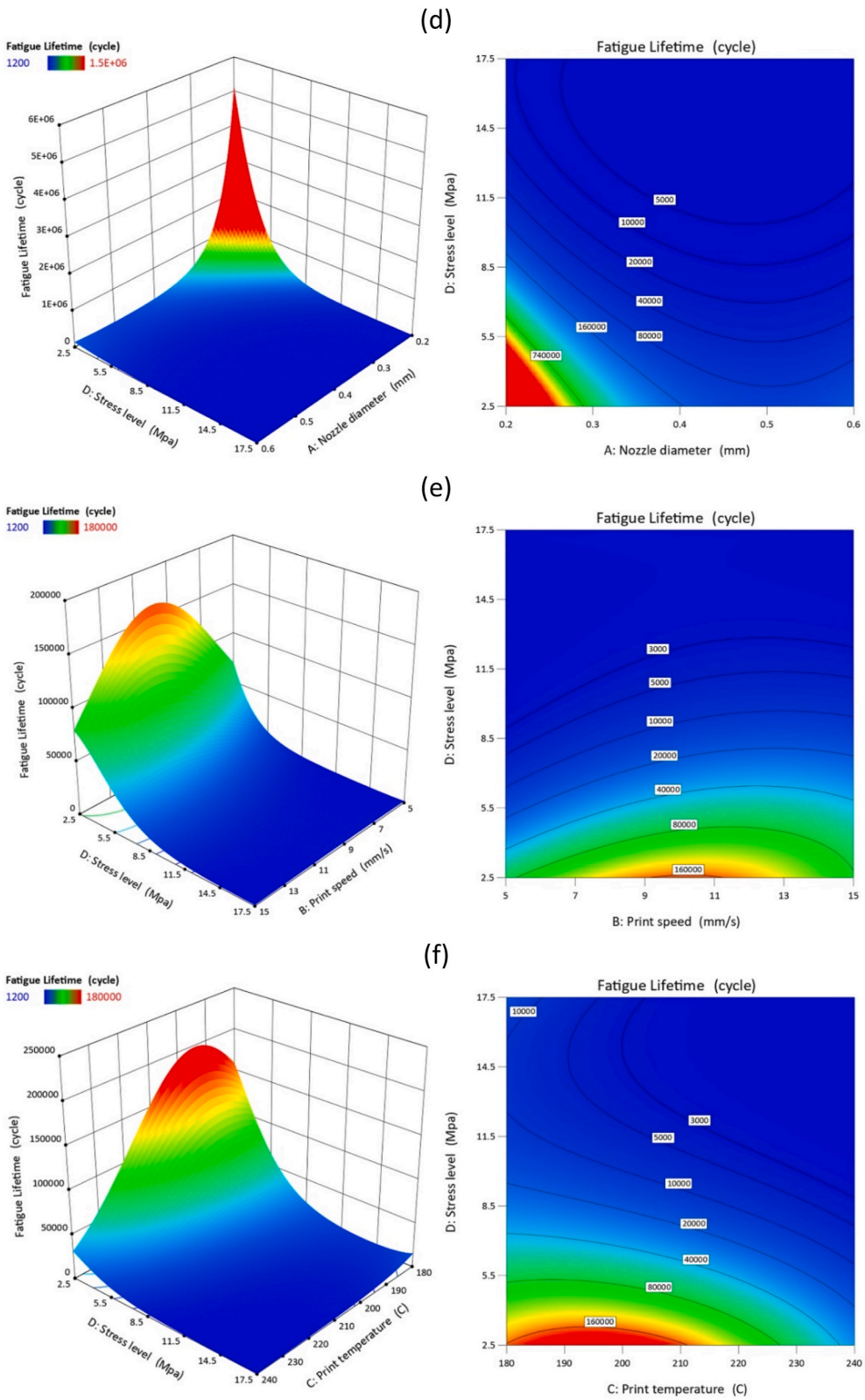


Fig. 13. (continued).

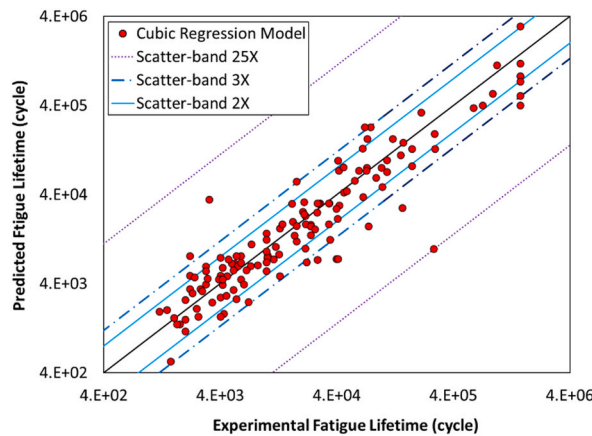


Fig. 14. The scatter-band analysis of the confirmation data.

provide a clearer insight of the model accuracy. It is worth considering for improving reliability.

3.4. Optimization

In order to find the optimum combination of parameters hill climbing technique was used. A multi-dimensional pattern search was performed using a penalty function. A small value as a starting point was selected in a downhill simplex and the searching process was carried out using a larger value until initial convergence when the changes of objective function compared to the previous iteration were smaller than 10^{-6} . Consequently, the table of the optimal sets of solutions is reported in Table 8.

A desirability of 1.00 shows that the goals can be reached quickly and better results may be available. Although a high desirability value is not the ultimate goal, it indicates that the results are acceptable. The desirability contours were compared according to different parameters in Fig. 15-a-f. The standard error is another option for choosing valuable predictions. This shows how far the range of factors can be extrapolated with low error.

Fig. 16 presents a plot where the ratio of the fatigue lifetime to the weight is compared to the ratio of the applied stress to the weight, based on the results of the fatigue tests (Fig. 16-a) and the predicted results (Fig. 16-b). As Pareto front is typically used for the multi-objective optimization, in this case, it was used to analyze the trade-off between the fatigue lifetime and the material strength. Therefore, there are two objectives and normalizing the data with the weight (an important parameter in additive manufacturing design [56]) can minimize the effect of cellular structures [57].

Nevertheless, by considering the maximum service lifespan as the main objective, the printing with 0.2 mm nozzle diameter, 5 mm/s printing speed, and 210 °C printing temperature leads to the optimum solution under a stress level of 2.5 MPa, based on Table 8.

3.5. Fractography

Failure analysis is a critical process in engineering designs that is performed to determine the causes that have led to an undesired loss of functionality. Therefore, the fracture surfaces of the test samples were prepared by coating with a thin conductive golden layer (by sputtering) and were inspected in the field-emission scanning electron microscopy (FE-SEM). As a note, according to the few areas of the fracture surfaces, due to their meta-structure, it may be difficult to determine the fracture mechanisms. The microscopic examination usually begins with low-magnification images. The infill pattern of the samples (rectilinear) and filling density (60%) are indicated in Fig. 17. As metamaterials are structured materials with exceptional characteristics, such structure results in lighter components, which is valuable advantage with wide-ranging applications, especially in the field of bio-printing. It should be noted that this is an optimized structure for best overall fatigue performance [29]. There were some changes in the line width of the raster paths, which can be due to inappropriate distance between the print head and the build platform, therefore the interaction between print heat and deposited layer [58]. Moreover, adjusting the print temperature can minimize the deviation from the designed dimensions [59].

Table 8

The optimal solutions for the numerical optimization process.

Nozzle Diameter (mm)	0.2	0.2	0.208	0.201	0.2
3D Printing Speed (mm/s)	8.711	5	12.466	5.779	5.141
3D Printing Temperature (°C)	207.423	210	236.132	215.235	180.332
Stress Level (MPa)	3.078	2.5	2.709	3.538	4.251
Fatigue Lifetime (cycle)	4128826	3116176	2584069	2247966	1876140
Standard Error	0.216	0.173	0.23	0.133	0.198
Desirability	1	1	1	1	1

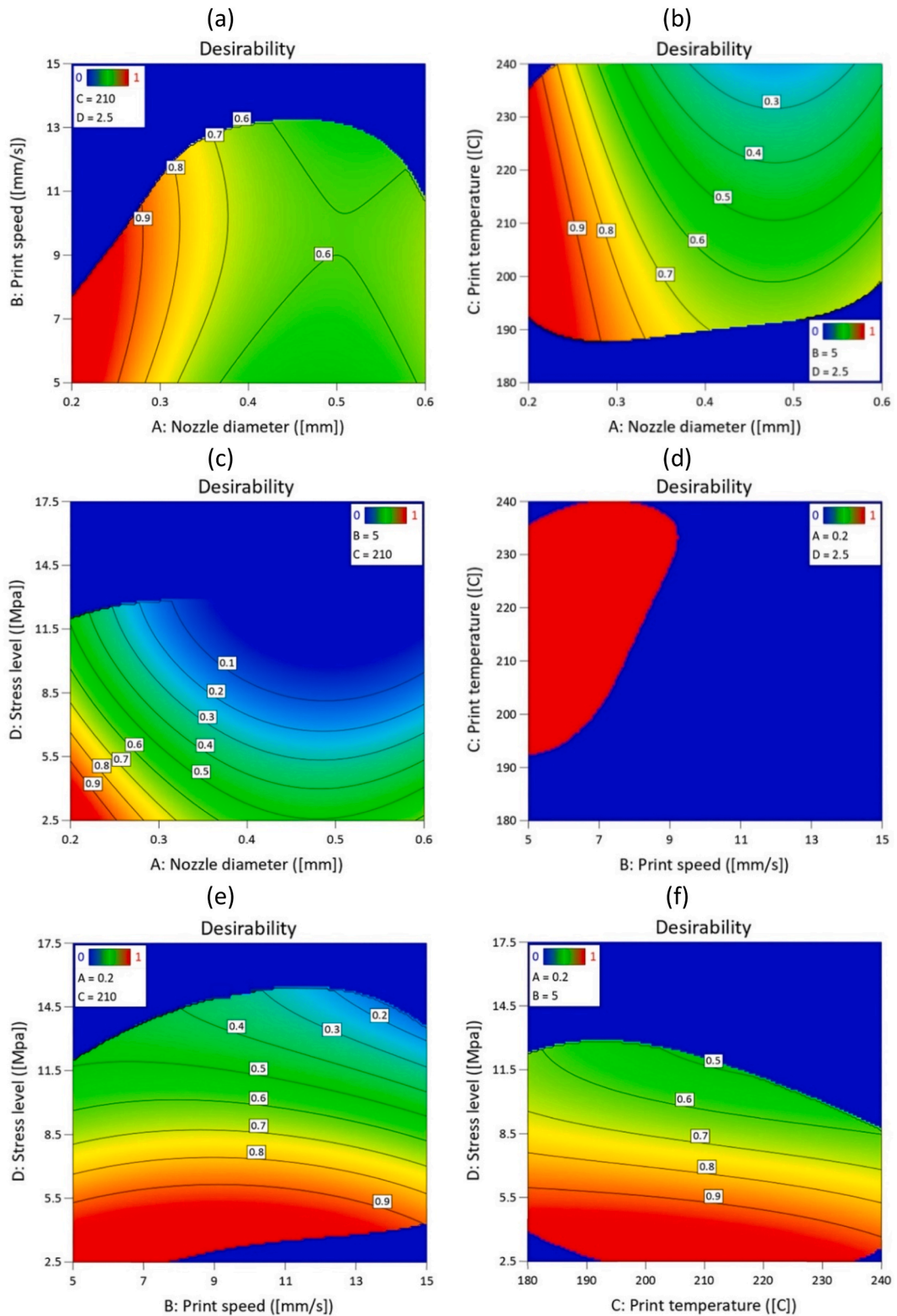


Fig. 15. Desirability changes in different values of design parameters.

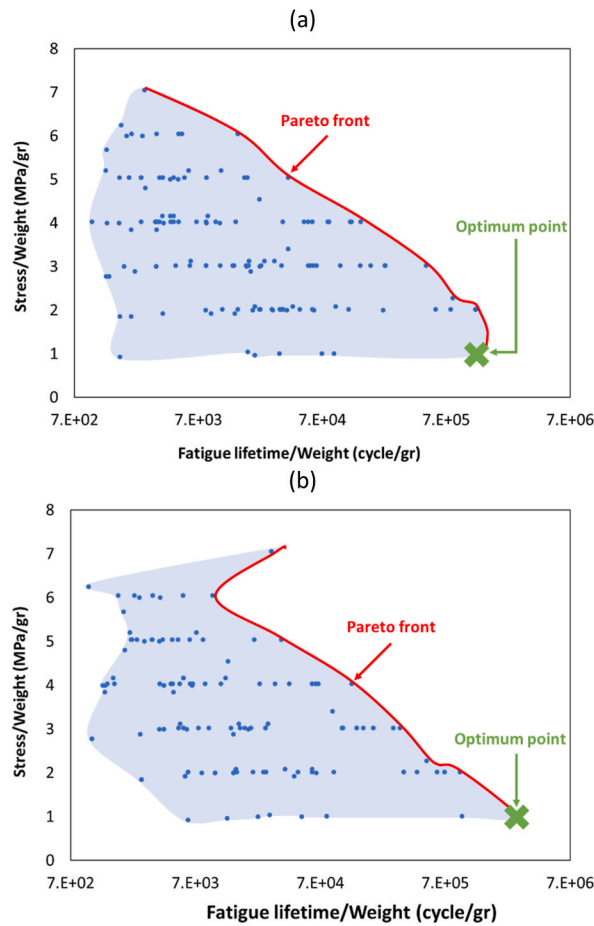


Fig. 16. The Pareto front curves for (a) experimental data and (b) regression results.

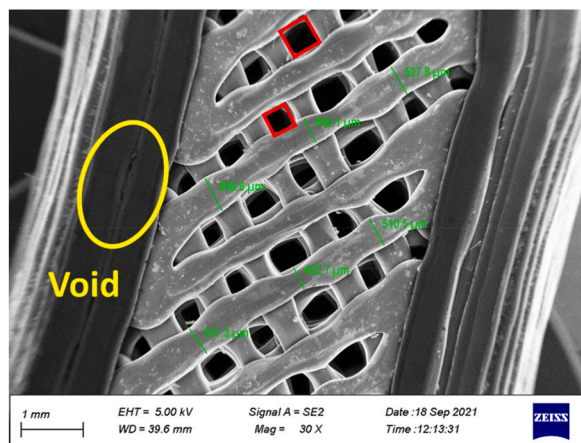


Fig. 17. The cross-section of the printed sample (PLA-0.6-10-180).

These changes can lead to voids that reduce the determined filling density and consequently, the strength of the material will decrease [34].

In general, fatigue failures have one or more fatigue origins from which the crack nucleates (Stage I). Fatigue crack initiation sites include surface defects such as voids, notches, or other geometric changes, which can act as stress concentrators and produce micro-cracks (Fig. 18-a). Such defects may occur during the filament fabrication process, through extrusion during the print process, or with

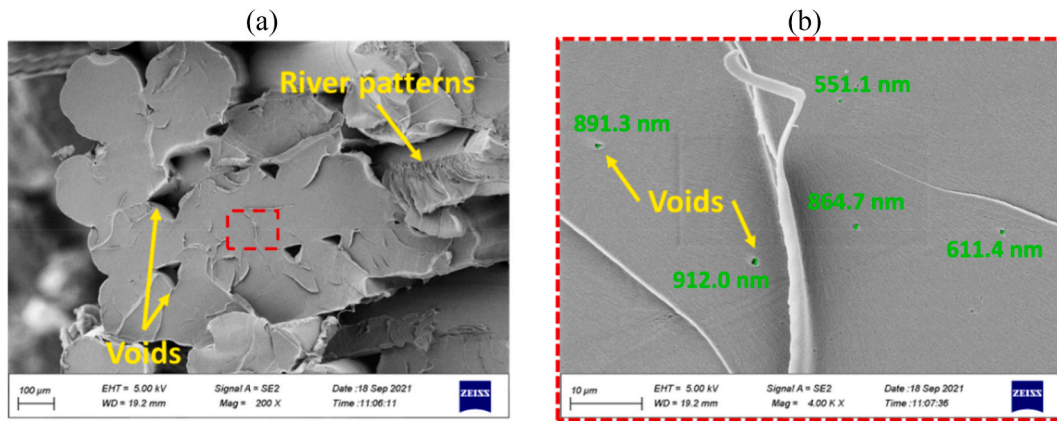


Fig. 18. The microscopic defects observed within the samples (PLA-0.2-15-180).

inappropriate speed and precision in the nozzle movement (Fig. 18-b). The plastic deformation resulting from this stress concentration, along with the increase in nominal stresses near the free surfaces, causes the accumulation of damage in these areas [58]. Moreover, based on the observations in Fig. 19-a and Fig. 19-b the surfaces in contact with support material have a worth surface finish than the free surfaces which can act as crack nucleation sites [60].

Subsequently, the fatigue cracks propagate gradually through the cross section (Stage II). The cleavage features containing flat facets in this area indicate a low-energy fracture, as depicted in Fig. 20-a. On the other hand, the plateaus on which the fatigue crack propagates are joined by the tear ridges. The fracture is caused by the gradual joining of active cleavage planes, which form a network of cleavage steps, known as a river pattern [16].

As the magnitude of each cycle in fatigue loading cannot cause a complete fracture of the component, the crack propagates progressively until a critical size when the complete fracture ensues. Such a gradual process leaves a series of parallel lines on the fracture surface radiating away from the origin. These progression marks are called beach marks and are resolved into a series of concentric arcs at higher magnifications, namely fatigue striations. Sometimes, several distinct periodic parallel marks are also observed on the fatigue fracture surfaces which can be caused by the impression of a particle or protrusion during the closing portion of the loading cycle. These are known as tire tracks due to their striking resemblance to the tracks left by tire tread as shown in Fig. 21-b. Such marks describe an out-of-plane shear (mode III) in loading conditions [61].

According to the obtained evidence, the failure of polylactic acid is a brittle phenomenon. This claim can be supported by the literature on the properties of polylactic acid [62]. However, the formation of fibrillated structures (Fig. 20-b, Fig. 21-b) called crazing, is a plastic mechanism that can be easily observed in transparent plastics [63]. The craze is a cracklike planar defect that contains a network of micro-voids among highly drawn polymer fibrils bridging the interfaces (Fig. 22-a). The craze deforms under the hydrostatic tension component of the stress tensor, which leads to the elongation of the fibrils along the direction of the maximum principal tensile stress. By exceeding the longitudinal strain in fibrils from maximum extensibility, they rupture and cause crack formation [64]. The craze formation has been reported to be associated with heat generation [63], however, the temperature was not measured through testing in this study. In the end, the crack growth rate increases significantly and becomes unstable when its length reaches a threshold value. This is stage III of the fatigue crack growth process that leads to the final fracture and occurs during the last loading cycle [65].

Crazes act as stress concentrators and initiate cracks at their tips or along their boundaries. The cracks propagate along the direction of the applied stress, leading to the brittle fracture. The fatigue properties of plastics are influenced by the number and size of crazes, as well as the rate of crack growth. Crazes can also coalesce and form larger cracks, which reduce the load-bearing capacity of the material. The fatigue lifetime of a plastic material is defined as the number of cycles of stress or strain that it can withstand before failure. The fatigue lifetime is affected by the frequency, amplitude, waveform, and mean value of the applied stress or strain, as well as the temperature and environmental conditions [66]. Therefore, crazing is an important factor to consider when designing plastic products or components that are subjected to cyclic loading or environmental stress. Crazing can be prevented or reduced by improving the molecular structure and morphology of the polymers, increasing its toughness and ductility, adding reinforcements or fillers, applying protective coatings or treatments, or reducing the exposure to solvents or other agents that can induce crazing [64].

In addition, the comparison of fracture surfaces at different print temperatures in Fig. 23-a-c illustrates the regularity of the layers is higher in the samples printed at 180 °C and decreases with increasing temperature. The layer regularity can improve the mechanical properties. A similar result has been obtained in work by Duan et al. [67] for foams made of PLA with a 3D printer. Along with the crack growth, the deformation increases, and more elongated fibers are formed [64].

To study the impact of nozzle diameter on the fracture mechanism, samples printed at a speed of 15 mm/s and a temperature of 180 °C were compared with different nozzle diameters in Fig. 24-a-c. The sample with a diameter of 0.4 mm has more plastic deformation, therefore, absorbs more energy to fail [64]. This plastic deformation is reduced in nozzle diameter of 0.6, 0.2, respectively, due to the enlargement of the cleavage plates.

According to the microscopic images, this is exacerbated at fracture surfaces, as print speed increases. The craze interfaces were not

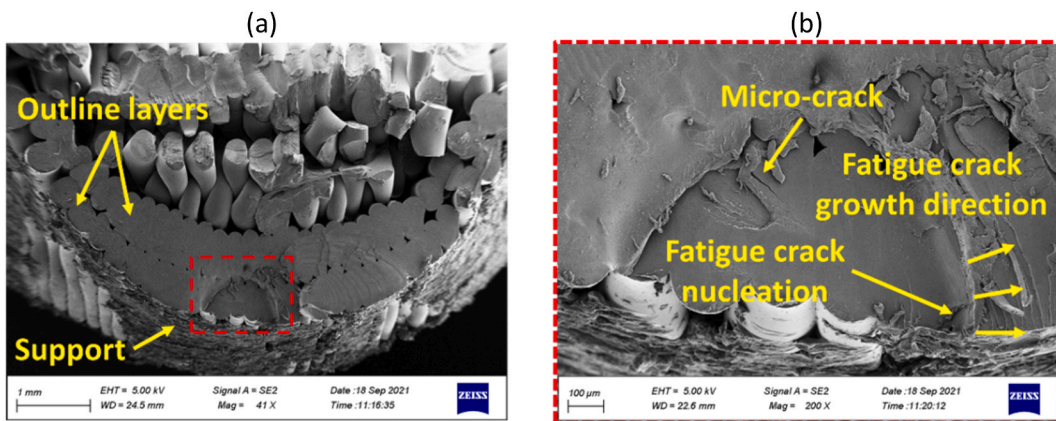


Fig. 19. Fatigue failure process of a specimen (PLA-0.6-10-180).

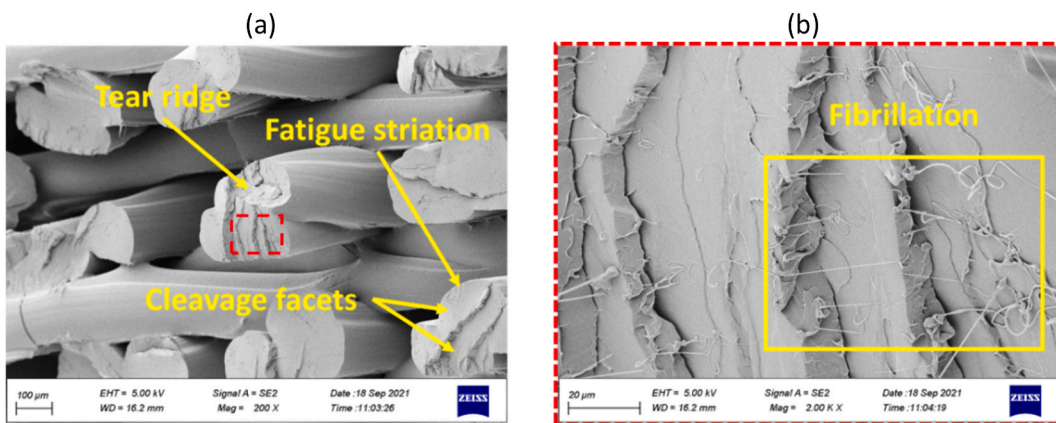


Fig. 20. Features of fracture surface (PLA-0.2-15-180).

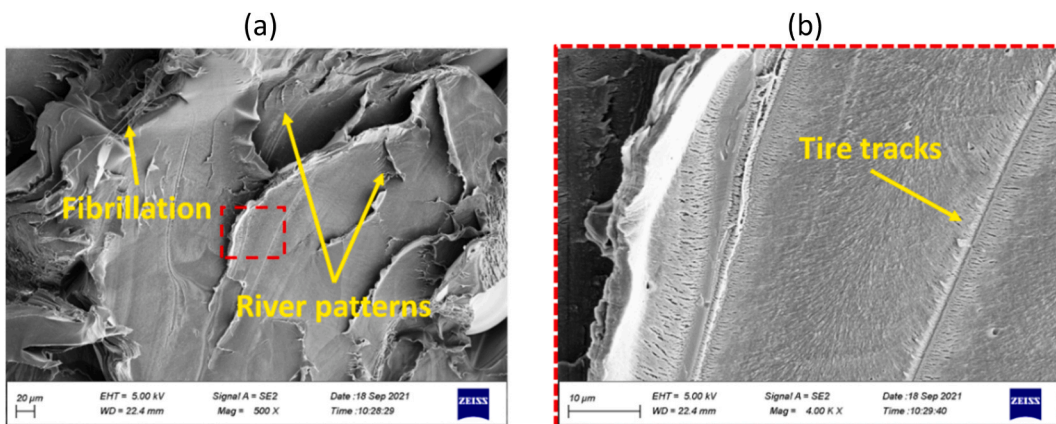


Fig. 21. Tire tracks on fatigue fracture surface (PLA-0.2-15-240).

separated in samples with a print speed of 5 mm/s in Fig. 22-b. In the case of samples manufactured with a print speed of 10 mm/s, Fig. 25-a, the diameter of the fibers was measured as 480 nm, on average. This is while, on the fracture surface corresponding to the print speed of 15 mm/s, the average diameter has decreased to 168 nm (Fig. 25-b).

The FE-SEM examination of fracture surfaces provides invaluable insights, as it demonstrates the factors behind functionality loss. These findings significantly contribute to both additive manufacturing by enhancing our understanding of structural failures. They

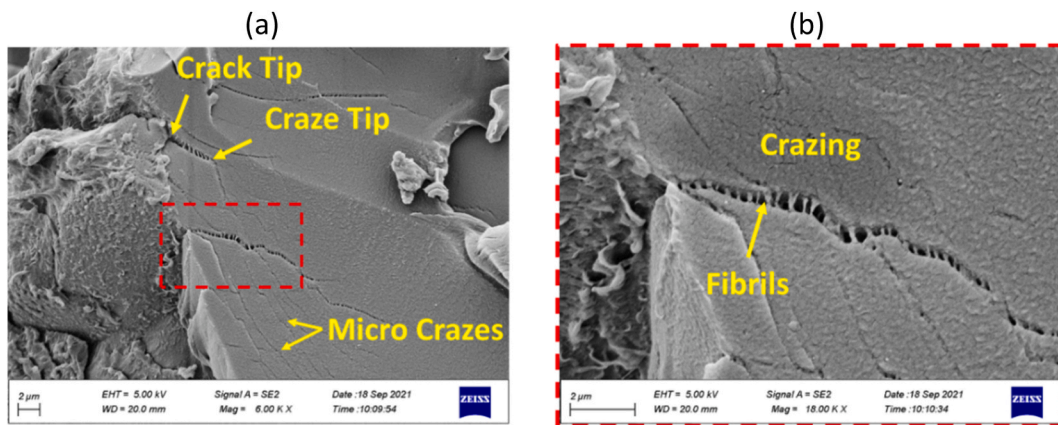


Fig. 22. Crazing and fiber bridging in crack formation (PLA-0.2-5-180).

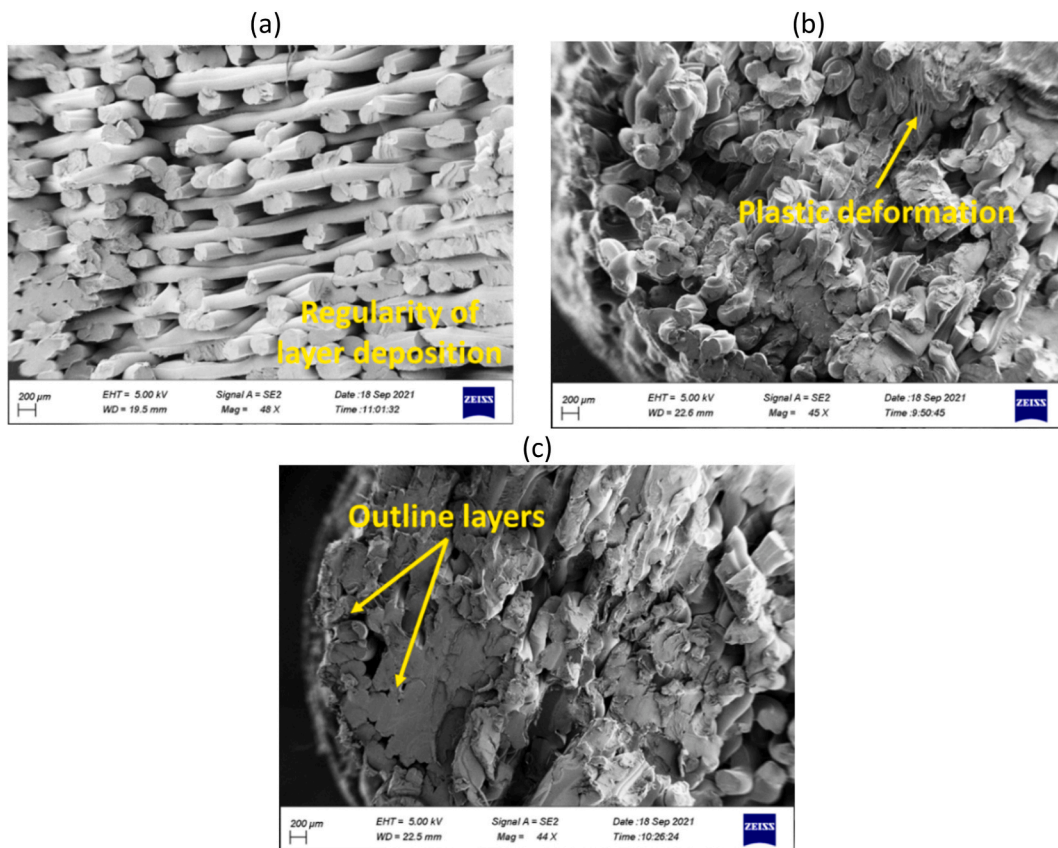


Fig. 23. The regularity of layers in samples printed with the print temperature of (a) 180 °C (PLA-0.2-15-180), (b) 210 °C (PLA-0.2-15-210), and (c) 240 °C (PLA-0.2-15-240).

provide knowledge to better understanding of material response under different conditions of manufacturing processes, ultimately leading to the design of higher-performance and more reliable components, which is a fundamental advancement in these fields.

4. Conclusions

The influence of 3D printing process parameters on the high-cycle fatigue behaviors of polylactic acid (PLA) material was investigated in this article. For this purpose, standard samples were additively manufactured with a print speed of 5, 10, and 15 mm/s, at 180, 210, and 240 °C as print temperature, with a nozzle diameter equal to 0.2, 0.4, and 0.6 mm using fused deposition modeling 3D

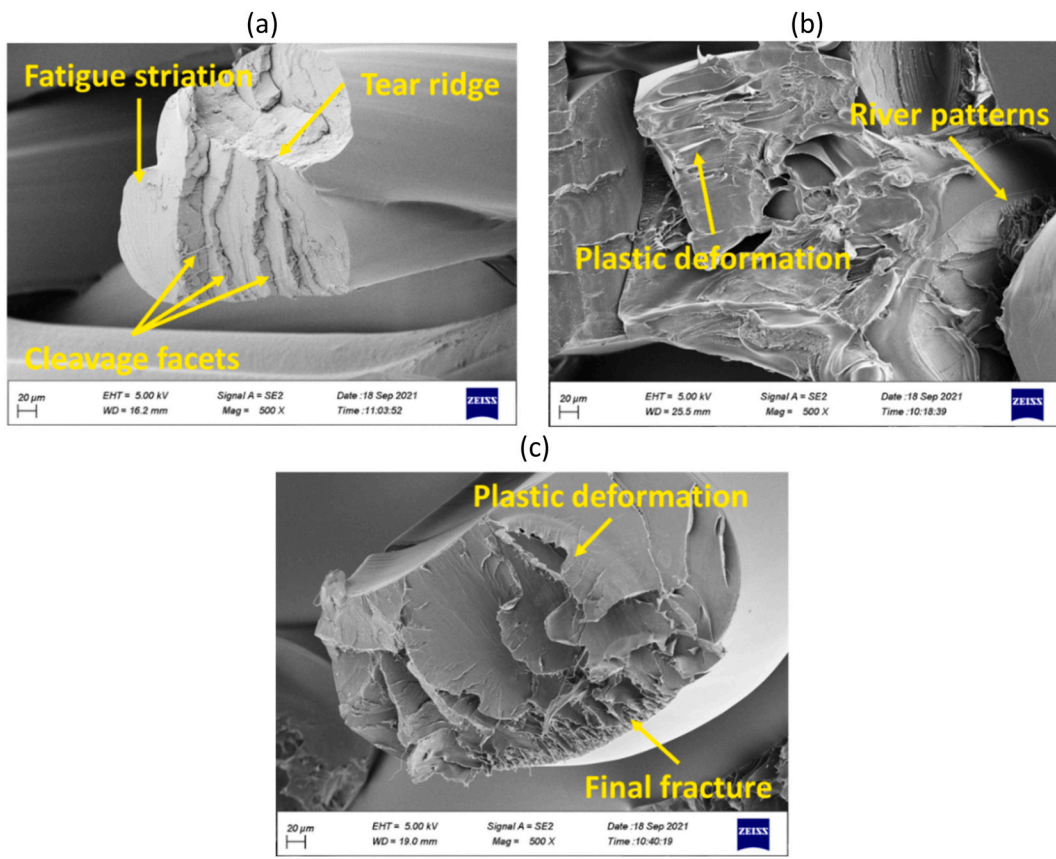


Fig. 24. The regularity of layers in samples printed with the nozzle diameter of (a) 0.2 mm (PLA-0.2-15-180), (b) 0.4 mm (PLA-0.4-15-180), and (c) 0.6 mm (PLA-0.6-15-180).

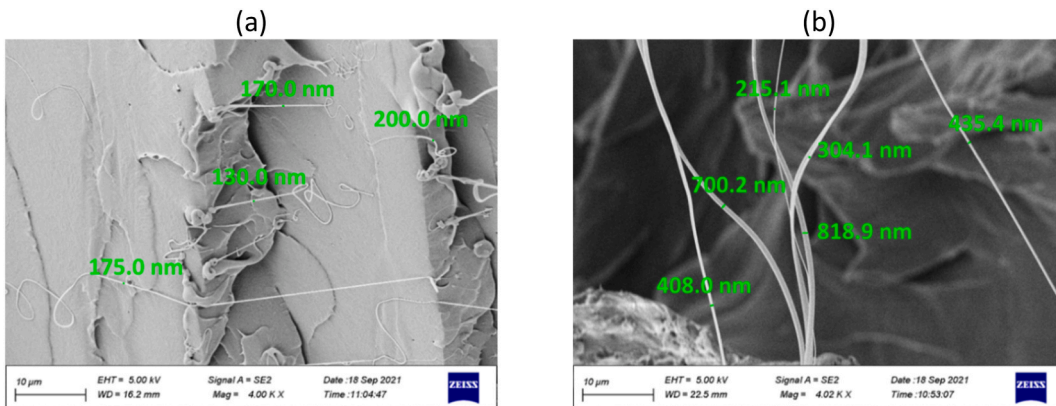


Fig. 25. The measured diameter of the fibers in the sample with a print speed of (a) 10 mm/s (PLA-0.2-10-180) and (b) 15 mm/s (PLA-0.2-15-180).

printer. After performing the rotary bending fatigue tests, the fracture surfaces of the specimens were inspected with a field-emission scanning electron microscopy (FE-SEM) to determine the failure mechanisms. Moreover, the material behavior was explained using a cubic equation. The results were as follows.

- By comparing the S–N curves resulting from the rotary bending fatigue tests, it is concluded that the print speed affects the low cycle behavior of the material. Still, the influence was different according to the other parameters. Generally, increasing the nozzle diameter decreased the resistance of the specimens significantly, which can be due to the inappropriate ratio of layer thickness to nozzle diameter. However, the lower print temperature results in more fatigue lifetime.

- A cubic model was fitted on 75% of the test results using regression analysis and confirmed with the remaining quarter of the data. The stress level, print speed, print temperature, and nozzle diameter were considered as design parameters to fit the fatigue lifetime. In the model, the R^2 value was 92.34%, all the main parameters were significant, and the corresponding P-value was less than 0.05. Moreover, R_{adj}^2 equal to 89.09% shows the model ability to predict the response properly. It was in reasonable agreement with R_{pred}^2 of 81.83%, and the difference was less than 20%. Nozzle diameter had no interaction with print temperature and stress level. This is while the other parameters had a clear interaction with each other, according to the corresponding graphs.
- Fatigue failure occurs in three stages. In the first stage, the crack was nucleated from the micro-cracks and the defects created during filament fabrication or in the sample manufacturing process. Further, with the growth of the fatigue crack, the striation lines have remained on the fracture surfaces. In the third stage, the final failure occurs, which is a fast and unstable phenomenon. Cleavage facets and river patterns can be the reason for the brittle behavior of the material. However, micro-crazing, which is a plastic mechanism, was observed in fractography. By increasing the printing speed, the diameter of the fibers decreased. In addition, at lower temperatures, the regularity of the layer deposition was higher. The plastic deformation in the samples printed with nozzle diameters of 0.4, 0.6, and 0.2 mm decreased, respectively.

Additive manufacturing is a rapidly evolving method for manufacturing complex parts. Despite the provision of multiple degrees of freedom by changing different print parameters, each of the parameters, individually or in interaction with other parameters, has a different effect on the final product, which must be considered in order to design safely and take advantage of the potential benefits of additive manufacturing. Incorrect process parameters cause defects in parts. Therefore, it is suggested that designers and engineers research the following topics.

- The effect of frequency on fatigue of additively manufactured components
- Thermal failure and the heat produced due to cyclical mechanical loading
- Post-processing and finishing methods in additive manufacturing
- Build process simulations to minimize the risk of part failure
- Using break-away support material with different polymers
- Investigating the effect of the ratio of the nozzle diameter to the layer thickness
- Development of a standard mechanical test method for additively manufactured parts in order to create a basis for producing more reliable and safer parts

Data availability

The experimental data could be found at Mendeley Data (Mohammad Azadi and Ali Dadashi, HCF testing raw data on 3D-printed PLA polymers, Volume 1, 2021) with the DOI number of 10.17632/gyxsn7wg6c.1, as well as Azadi, Mohammad; Dadashi, Ali, "Experimental fatigue dataset for additive-manufactured 3D-printed Polylactic acid biomaterials under fully-reversed rotating-bending loadings", Data in Brief, Vol. 41, 107846, 2022, <https://doi.org/10.1016/j.dib.2022.107846>.

Funding

This study was financially supported by the Ministry of Science, Research, and Technology [the grant number: 16-99-01-000194, 2021], in Iran.

CRedit authorship contribution statement

Ali Dadashi: Writing – original draft, Visualization, Software, Resources, Methodology, Investigation, Formal analysis, Data curation. **Mohammad Azadi:** Writing – review & editing, Validation, Supervision, Resources, Project administration, Methodology, Investigation, Funding acquisition, Conceptualization.

Declaration of competing interest

The authors declare that they have no known competing financial interests or personal relationships that could have appeared to influence the work reported in this paper.

References

- [1] No. 52900, Additive Manufacturing – General Principles – Terminology, International Organization for Standardization, Standard, 2015, p. 2015.
- [2] S. Yuan, S. Li, J. Zhu, Y. Tang, Additive manufacturing of polymeric composites from material processing to structural design, *Compos. B Eng.* 219 (2021) 108903.
- [3] R.M. Walser, Metamaterials: an introduction, in: Werner S. Weiglhofer, A. Lakhtakia (Eds.), *Introduction to Complex Mediums for Optics and Electromagnetics*, SPIE Publications, 2003.
- [4] A. Clausen, F. Wang, J.S. Jensen, O. Sigmund, J.A. Lewis, Topology optimized architectures with programmable Poisson's ratio over large deformations, *Adv. Mater.* 27 (37) (2015) 5523–5527.
- [5] S. Sepehri, H. Jafari, M.M. Mashhadi, M.R.H. Yazdi, M.M.S. Fakhraabadi, Study of tunable locally resonant metamaterials: effects of spider-web and snowflake hierarchies, *Int. J. Solid Struct.* 204 (205) (2020) 81–95.

- [6] Z. Yang, Q. Liang, Y. Duan, Z. Li, D. Li, Y. Cao, A 3D-printed lightweight broadband electromagnetic absorbing metastructure with preserved high-temperature mechanical property, *Compos. Struct.* 274 (2021) 114330.
- [7] J. Fan, L. Zhang, S. Wei, Z. Zhang, S.K. Choi, B. Song, Y. Shi, A review of additive manufacturing of metamaterials and developing trends, *Mater. Today* 50 (2021) 303–328.
- [8] C. Abeykoon, P. Sri-Amphorn, A. Fernando, Optimization of fused deposition modeling parameters for improved PLA and ABS 3D printed structures, *International Journal of Lightweight Materials and Manufacture* 3 (3) (2020) 284–297.
- [9] A. Alafaghani, A. Qattawi, Investigating the effect of fused deposition modeling processing parameters using Taguchi design of experiment method, *J. Manuf. Process.* 36 (2018) 164–174. June.
- [10] G.S. Sandhu, K.S. Boparai, K.S. Sandhu, Effect of slicing parameters on surface roughness of fused deposition modeling prints, *Mater. Today: Proc.* 48 (2022) 1339–1345.
- [11] G.S. Sandhu, K.S. Boparai, K.S. Sandhu, Influence of slicing parameters on selected mechanical properties of fused deposition modeling prints, *Mater. Today: Proc.* 48 (2022) 1378–1382.
- [12] J. Antonio Travieso-Rodríguez, M.D. Zandi, R. Jerez-Mesa, J. Lluma-Fuentes, Fatigue behavior of PLA-wood composite manufactured by fused filament fabrication, *J. Mater. Res. Technol.* 9 (No. 4) (2020) 8507–8516.
- [13] P. Patil, D. Singh, S.J. Raykar, J. Bhamu, Multi-objective optimization of process parameters of Fused Deposition Modeling (FDM) for printing Poly(lactic Acid (PLA) polymer components, *Mater. Today: Proc.* 45 (2021) 4880–4885.
- [14] T. Cui, S. Mukherjee, P.M. Sudeep, G. Colas, F. Najafi, J. Tam, P.M. Ajayan, C.V. Singh, Y. Sun, T. Fillette, Fatigue of graphene, *Nat. Mater.* 19 (4) (2020) 405–411, 2020 19:4.
- [15] ASTM E1823, Standard Terminology Relating to Fatigue and Fracture, ASTM, West Conshohocken, PA, 2000, 03.01.
- [16] R.I. Stephens, A. Fatemi, R.R. Stephens, H.O. Fuchs, *Metal Fatigue in Engineering*, second ed., Wiley-Interscience, 2000.
- [17] G. Gomez-Gras, R. Jerez-Mesa, J.A. Travieso-Rodríguez, J. Lluma-Fuentes, Fatigue performance of fused filament fabrication PLA specimens, *Mater. Des.* 140 (2018) 278–285.
- [18] M.F. Afrose, S.H. Masood, P. Iovenitti, M. Nikzad, I. Sbarski, Effects of part build orientations on fatigue behaviour of FDM-processed PLA material, *Progress in Additive Manufacturing* 1 (No. 1) (2016) 21–28.
- [19] O.H. Ezeh, L. Susmel, On the notch fatigue strength of additively manufactured polylactide (PLA), *Int. J. Fatig.* 136 (2020) 105583.
- [20] H. Zhang, L. Cai, M. Golub, Y. Zhang, X. Yang, K. Schlarman, J. Zhang, Tensile, creep, and fatigue behaviors of 3D-printed acrylonitrile butadiene styrene, *J. Mater. Eng. Perform.* 27 (2018) 57–62.
- [21] J. Lee, A. Huang, Fatigue analysis of FDM materials, *Rapid Prototyp. J.* 19 (No. 4) (2013) 291–299.
- [22] M. Domingo-Espin, J.A. Travieso-Rodríguez, R. Jerez-Mesa, J. Lluma-Fuentes, Fatigue performance of ABS specimens obtained by fused filament fabrication, *Materials* 11 (No. 12) (2018) 2521.
- [23] S.H. Ahn, M. Montero, D. Odell, S. Roundy, P.K. Wright, Anisotropic material properties of fused deposition modeling ABS, *Rapid Prototyp. J.* 8 (No. 4) (2002) 248–257.
- [24] S.M. Esfarjani, A. Dadashi, M. Azadi, Topology optimization of additive-manufactured metamaterial structures: a review focused on multi-material types, *Forces in Mechanics* 7 (2022) 100100.
- [25] V. Shanmugam, O. Das, K. Babu, U. Marimuthu, A. Veerasimman, D.J. Johnson, R.E. Neisiany, M.S. Hedenqvist, S. Ramakrishna, F. Berto, Fatigue behaviour of FDM-3D printed polymers, polymeric composites and architected cellular materials, *Int. J. Fatig.* 143 (2021) 106007.
- [26] O.A. Mohamed, S.H. Masood, J.L. Bhowmik, Optimization of fused deposition modeling process parameters: a review of current research and future prospects, *Advances in Manufacturing* 3 (2015) 42–53.
- [27] M. Azadi, A. Dadashi, Experimental fatigue dataset for additive-manufactured 3D-printed Poly(lactic acid) biomaterials under fully-reversed rotating-bending loading, *Data Brief* 41 (2022) 107846.
- [28] A. Dadashi, M. Azadi, Experimental bending fatigue data of additive-manufactured PLA biomaterial fabricated by different 3D printing parameters, *Progress in Additive Manufacturing* 8 (2023) 255–263.
- [29] A. Dadashi, M. Azadi, Multi-objective numerical optimization of 3D-printed poly(lactic acid) bio-metamaterial based on topology, filling pattern, and infill density via fatigue lifetime and mass, *PLoS One* 18 (No. 9) (2023) e0291021.
- [30] J. Liao, N. Brosse, A. Pizzi, S. Hoppe, X. Zhou, G. Du, Characterization and 3D printability of poly(lactic acid)/acetylated tannin composites, *Ind. Crop. Prod.* 149 (2020) 112320.
- [31] J.C. Camargo, Á.R. Machado, E.C. Almeida, E.F.M.S. Silva, Mechanical properties of PLA-graphene filament for FDM 3D printing, *Int. J. Adv. Des. Manuf. Technol.* 103 (5) (2019) 2423–2443.
- [32] P. Geng, J. Zhao, Z. Gao, W. Wu, W. Ye, G. Li, H. Qu, Effects of printing parameters on the mechanical properties of high-performance poly(phenylene sulfide) three-dimensional printing, *3D Print. Addit. Manuf.* 8 (No. 1) (2021) 33–41.
- [33] W. Xu, A. Pranovich, P. Uppstu, X. Wang, D. Kronlund, J. Hemming, H. Öblom, N. Moritz, M. Preis, N. Sandler, S. Willför, C. Xu, Novel biorenewable composite of wood polysaccharide and poly(lactic acid) for three dimensional printing, *Carbohydr. Polym.* 187 (2018) 51–58.
- [34] V.E. Kuznetsov, A.N. Solonin, O.D. Urzhumtsev, R. Schilling, A.G. Tavitov, Strength of PLA components fabricated with fused deposition technology using a desktop 3D printer as a function of geometrical parameters of the process, *Polymers* 10 (No. 3) (2018) 313.
- [35] Z. Wang, J. Xu, Y. Lu, L. Hu, Y. Fan, J. Ma, X. Zhou, Preparation of 3D printable micro/nanocellulose-poly(lactic acid) (MNC/PLA) composite wire rods with high MNC constitution, *Ind. Crop. Prod.* 109 (2017) 889–896.
- [36] K. Zhao, D. Wang, K. Li, M. Da, R. Dharma Bintara, Z. Lubis, Y. Rohmat, A. Pradana, J. Wu, Study on optimization of 3D printing parameters, *IOP Conf. Ser. Mater. Sci. Eng.* 392 (No. 6) (2018) 062050.
- [37] D. Stoof, K. Pickering, Y. Zhang, Fused deposition modelling of natural fibre/poly(lactic acid) composites, *Journal of Composites Science* 1 (No. 1) (2017) 8.
- [38] M. Moradi, M.K. Moghadam, M. Shamsborhan, M. Bodaghi, The synergic effects of FDM 3D printing parameters on mechanical behaviors of bronze poly(lactic acid) composites, *Journal of Composites Science* 4 (No. 1) (2020) 17.
- [39] X. Tian, T. Liu, C. Yang, Q. Wang, D. Li, Interface and performance of 3D printed continuous carbon fiber reinforced PLA composites, *Compos. Appl. Sci. Manuf.* 88 (2016) 198–205.
- [40] E.O. Cisneros-López, A.K. Pal, A.U. Rodríguez, F. Wu, M. Misra, D.F. Mielewski, A. Kiziltas, A.K. Mohanty, Recycled poly(lactic acid)-based 3D printed sustainable biocomposites: a comparative study with injection molding, *Materials Today Sustainability* 7–8 (2020) 100027.
- [41] H.L. Tekinalp, X. Meng, Y. Lu, V. Kunc, L.J. Love, W.H. Peter, S. Ozcan, High modulus biocomposites via additive manufacturing: cellulose nanofibril networks as “microsponges,” *Compos. B Eng.* 173 (2019) 106817.
- [42] S. Yu, Y.H. Hwang, J.Y. Hwang, S.H. Hong, Analytical study on the 3D-printed structure and mechanical properties of basalt fiber-reinforced PLA composites using X-ray microscopy, *Compos. Sci. Technol.* 175 (2019) 18–27.
- [43] M. Heidari-Rarani, M. Rafiee-Afarani, A.M. Zahedi, Mechanical characterization of FDM 3D printing of continuous carbon fiber reinforced PLA composites, *Compos. B Eng.* 175 (2019) 107147.
- [44] ASM Handbook, Additive Manufacturing Processes, ume 24, ASM International, 2020.
- [45] ISO 1143, Metallic Materials - Rotating Bar Bending Fatigue Testing, ISO International Standard, 2010.
- [46] J.W. Comb, W.R. Priedeman, P.W. Turley, FDM® Technology process improvements, in: *International Solid Freeform Fabrication Symposium*, 1994.
- [47] O.H. Basquin, The exponential law of endurance tests, *American Society for Testing and Materials Proceedings* 10 (1910) 625–630.
- [48] J. Antoy, *Design of Experiments for Engineers and Scientists: 2nd Edition*, Elsevier Ltd, 2014.
- [49] M. Azadi, M. Alizadeh, H. Sayar, Sensitivity analysis for effects of displacement amplitude and loading frequency on low-cycle fatigue lifetime in carbon/epoxy laminated composites, *MATEC Web of Conferences* 165 (2018).
- [50] J. Paulo Davim, *Design of Experiments in Production Engineering*, Springer Cham, 2016.

- [51] W.A. Jensen, Confirmation runs in design of experiments, *A Quarterly Journal of Methods, Applications and Related Topics* 48 (No. 2) (2017) 162–177.
- [52] P. Wang, B. Zou, H. Xiao, S. Ding, C. Huang, Effects of printing parameters of fused deposition modeling on mechanical properties, surface quality, and microstructure of PEEK, *J. Mater. Process. Technol.* 271 (2019) 62–74.
- [53] D. Fischer, C. Ebbach, R. Schönherr, D. Dietrich, D. Nickel, Improving inner structure and properties of additive manufactured amorphous plastic parts: the effects of extrusion nozzle diameter and layer height, *Addit. Manuf.* 51 (2022) 102596.
- [54] A.A. Ansari, M. Kamil, Effect of print speed and extrusion temperature on properties of 3D printed PLA using fused deposition modeling process, *Mater. Today: Proc.* 45 (2021) 5462–5468.
- [55] S. Ding, B. Zou, P. Wang, H. Ding, Effects of nozzle temperature and building orientation on mechanical properties and microstructure of PEEK and PEI printed by 3D-FDM, *Polym. Test.* 78 (2019) 105948.
- [56] M. Azadi, A. Dadashi, M.S. Aghareb Parast, S. Dezianian, A. Bagheri, A. Kami, M. Kianifar, Vahid Asghari, A comparative study for high-cycle bending fatigue lifetime and fracture behavior of extruded and additive-manufactured 3D-printed acrylonitrile butadiene styrene polymers, *International Journal of Additive-Manufactured Structures* 1 (No. 1) (2022) 1–14.
- [57] S.M.F. Kabir, K. Mathur, A.F.M. Seyam, Impact resistance and failure mechanism of 3D printed continuous fiber-reinforced cellular composites, *J. Text. Inst.* 112 (No. 5) (2021) 752–766.
- [58] B.N. Turner, R. Strong, S.A. Gold, A review of melt extrusion additive manufacturing processes: I. Process design and modeling, *Rapid Prototyp. J.* 20 (No. 3) (2014) 192–204.
- [59] S. Singamneni, M.P. Behera, D. Truong, M.J. Le Guen, E. Macrae, K. Pickering, Direct extrusion 3D printing for a softer PLA-based bio-polymer composite in pellet form, *J. Mater. Res. Technol.* 15 (2021) 936–949.
- [60] O. Diegel, A. Nordin, D. Motte, *A Practical Guide to Design for Additive Manufacturing*, Springer Singapore, Singapore, 2019.
- [61] *ASM Handbook Volume 12: Fractography*, ASM International, 1987.
- [62] L.T. Sin, B.S. Tveen, *A Practical Guide for the Processing, Manufacturing, and Applications of PLA*, second ed., *Plastics Design Library*, 2019.
- [63] Z. Yang, J. Zhang, Z. Zhu, C. Jiang, Q. Cheng, H. Jiang, Mechanism of temperature rise due to crazing evolution during PMMA scratch, *Int. J. Solid Struct.* 199 (2020) 120–130.
- [64] *ASM Handbook, Volume 11: Failure Analysis and Prevention*, ASM International, 2002.
- [65] P. Cavaliere, *Fatigue and Fracture of Nanostructured Materials*, Springer International Publishing, 2021.
- [66] Y. Yan, Y. Sun, J. Su, B. Li, P. Zhou, Crazing initiation and growth in polymethyl methacrylate under effects of alcohol and stress, *Polymers* 15 (No. 6) (2023) 1375.
- [67] Y. Duan, B. Du, X. Zhao, N. Hou, X. Shi, B. Hou, Y. Li, The cell regularity effects on the compressive responses of additively manufactured Voronoi foams, *Int. J. Mech. Sci.* 164 (2019) 105151.